Network pharmacology approach and experimental verification of salidroside in the treatment of hepatocellular carcinoma

Bing Jiang
Gansu University of Traditional Chinese Medicine
Shiqi Huang
Gansu University of Traditional Chinese Medicine
Xuefei Bai
Gansu Provincial Cancer Hospital
Lele Tian
Gansu University of Traditional Chinese Medicine
Yanru Wang
Gansu University of Traditional Chinese Medicine
Tao Yang
Gansu University of Traditional Chinese Medicine
Longfei Feng
Gansu University of Traditional Chinese Medicine
Wenjing Guo
Gansu University of Traditional Chinese Medicine
Yangyang Li
Gansu University of Traditional Chinese Medicine
Xin Feng
Gansu University of Traditional Chinese Medicine
Tao Wang
Gansu Provincial Academic Institute for Medical Research, Gansu Provincial Cancer Hospital
Huan Guo
Gansu Provincial Academic Institute for Medical Research, Gansu Provincial Cancer Hospital
Haixiang Su (SHXsuhaixiang54120@163.com)
Gansu Provincial Academic Institute for Medical Research, Gansu Provincial Cancer Hospital

---

Research Article

Keywords: Network pharmacology, Salidroside, Chloroquine diphosphate, Autophagy, PI3K/AKT/mTOR

Posted Date: December 6th, 2023

DOI: https://doi.org/10.21203/rs.3.rs-3696850/v1

Additional Declarations: No competing interests reported.

Abstract

Background

Salidroside (Sal) is a bioactive component extracted from the rhizome of *Rhodiola rosea* L. Pharmacological studies have shown that Sal has good anti-cancer properties in various cancers, but the exact mechanism is not clear.

Method

This study validated the efficacy and explored the potential mechanisms of Sal in treating hepatocellular carcinoma (HCC) by integrating network pharmacology analyses and experimental verification. The pharmacological effects and molecular mechanism of Sal on HCC were explored by network pharmacology approach. HepG2 cells were treated with Sal and/or chloroquine diphosphate (CQ). The cell counting kit-8 (CCK-8) assay, inverted microscope (IM) observation, transmission electron microscope (TEM) observation, various staining were used to detect the condition of autophagy and apoptosis, and the western blotting was used to detect related proteins. Moreover, Sal and/or CQ was also used to treat HCC mice, the hematoxylin and eosin (H & E) staining was used to observe the pathological change of tumor tissue, the immunohistochemistry and western blotting were used to detect the change of related proteins in tumor tissue.

Results

The network pharmacology approach successfully identified that Sal might adjust autophagy flux through PI3K/AKT/mTOR pathway, which might affect the occurrence and development of HCC. The in vitro experiments indicated that Sal induced HepG2 cells autophagy and apoptosis. The in vitro and vivo experiments indicated that inhibition of autophagy promoted mitochondrial damage and apoptosis induced by Sal. Moreover, Caspase cascade reactions might be involved in these processes, especially the increased expression of cleaved-caspase-3 and cleaved-caspase-9. Notably, Sal also inhibited the activation of PI3K/AKT/mTOR pathway, while CQ promoted the activation of this pathway.

Conclusion

These findings provide important view for the molecular mechanism of interaction between autophagy and apoptosis, and also provide new insights for monitoring, diagnosis and treatment of HCC.

Introduction

According to the statistics of global cancer in 2023, hepatocellular carcinoma (HCC) is the sixth most universal cancer and the third most universal cause of cancer death in the world [1]. With the deepening

research of HCC, the methods of treatment have also developed rapidly. Following traditional surgery, radiotherapy and chemotherapy, new methods of treatment (such as interventional therapy, molecular targeted therapy, immunotherapy and cell therapy) have been widely applied in the treatment of HCC [2–4]. However, the prognosis of most patients remains still very poor, which is associated with the poor response of regimens for treatment [5], many side effects (consisting of gastrointestinal reaction, cutaneous pruritus and so on) [6] and multi-drug resistance [7]. Therefore, exploring effective and safe drugs for the treatment of HCC is still an urgent clinical problem.

Inducing apoptosis of cancer cells is one of the goals of anti-cancer effects. Apoptosis is an active physiological response and the main form of type I programmed cell death, which is identified by eversion of membrane, condensation of nuclear chromatin, split of nucleus and formation of apoptotic bodies [8]. Autophagy is a pathway of type II programmed cell death, which is different from apoptosis. Autophagy mainly refers to that autophagic vesicle can wrap senescent or damaged organelles by its double-layered membrane to form autophagosomes when cells are received some stimuli (such as starvation or hypoxia), and then autophagosomes combine with lysosomes to form autolysosomes, which can degrade the wrapped substances to maintain the stability of internal environment and the renewal of organelles [9]. When autophagy is interdicted, the mechanism of cellular survival may be inhibited. For example, Wang Yue *et al.* [10] have confirmed that pseudolaric acid B can induce autophagy and inhibit apoptosis in human lung fibroblasts MRC5 cells through the response of DNA damage. Autophagy can also produce some products (such as fatty acids, amino acids and so on), which provide nutrients for the growth of tumor [11, 12]. Furthermore, excessive autophagy may cause autophagic cell apoptosis. For example, resveratrol can synergistically treat ovarian cancer by inducing autophagy in human ovarian cancer cells [13]. The combined treatment of matrine and 5-fluorouracil can up-regulate the expression levels of autophagy-related genes ATG5 and Beclin-1 to enhance its chemosensitivity [14]. Thus, the cross-interference between autophagy and apoptosis remains still controversial.

Recently, autophagy has gradually become a hot topic in the territory of anti-cancer therapy. More and more researches shown that certain pharmaceutical ingredients, which are extracted from natural Chinese medicine, can also treat cancer through the pathway of autophagy. For example, ginsenoside F2 induces autophagy by up-regulating the expressions of ATG7, Beclin-1, and LC3B proteins in human breast cancer stem cells, and induces apoptosis by triggering the pathway of mitochondrial apoptosis, while the combined treatment of autophagy inhibitor chloroquine can enhance the ginsenoside F2-induced apoptosis [15]. Pulsatilla saponin D induces autophagy by increasing the level of p-ERK protein and decreasing the levels of p-mTOR and p-p70S6K proteins, while enhances the activity of anti-human cervical cancer HeLa cells [16].

Autophagy and apoptosis may play a key role in cancer [17]. More and more reports have shown that autophagy has a dual properties. Autophagy protects cells from various damaging factors, such as hypoxia or starvation, thus maintaining the stability of intracellular environment. In addition, autophagy can also promote apoptosis related to various cancers [18]. However, the molecular mechanism of cross-

intervention between autophagy and apoptosis is still unclear. Therefore, the purpose of this study is to explore the relationship between autophagy and apoptosis of HepG2 cells induced by salidroside (Sal), which a primary component extracted from the rhizome of *Rhodiola rosea* L. The results proved that autophagy might provide survival strategy for HepG2 cells by inhibiting apoptosis, while inhibiting autophagy could accelerates the apoptotic process of HepG2 cells. Our research may be helpful to elucidate the potential molecular mechanism of the cross-interference between autophagy and apoptosis in the stress-stimulated environment, which may be helpful to develop new therapy for liver cancer.

Materials and methods

Bioinformatic analysis

Acquisition of drug-relevant gene targets

In this study, the bioinformatics analysis tool BATMAN-TCM (a bioinformatics analysis tool for molecular mechanism of traditional Chinese medicine) database (http://bionet.ncpsb.org.cn/batman-tcm/), TCMSP database (https://old.tcmsp-e.com/tcmsp.php), Herb database (http://herb.ac.cn/), ETCM database (http://www.tcmip.cn/ETCM/index.php/Home/Index/), and the existing literature were used to collect the chemical composition of *Rhodiola rosea* L. The score given by the BATMAN-TCM database target prediction method was set to score cutoff ≥ 20, the adjusted P-value corrected by the Benjamini-Hochberg multiplex test was cut off to 0.05. And in the TCMSP database, the oral bioavailability (OB) value was set to ≥ 30%, the drug-like (DL) value was set to ≥ 0.18, the active ingredients of *Rhodiola rosea* L. and the relevant gene targets corresponding to the active ingredients were screened out in combination with the existing literature.

Acquisition of disease-associated gene targets

In the GeneCards database (https://www.genecards.org/), OMIM database (https://omim.org/) and DisGeNET database (https://www.disgenet.org/home/), “liver cancer”, as the keyword, was entered to retrieve the gene targets acting on liver cancer. After the duplicate numeric values were removed, so as to obtain relevant gene targets for the treatment of liver cancer.

Acquisition of targets for the intersection between drugs and diseases

The screened drug-related gene targets and disease-related gene targets were intersected to obtain the gene targets of Rhodiola rosea and Sal for the treatment of liver cancer, and the venn diagram of the intersection of the two was made by using the online software microbiotic information platform (http://www.bioinformatics.com.cn/), so as to facilitate the use of subsequent analysis.

Construction of a “traditional Chinese medicine-active ingredients-diseases-potential targets” network

The gene targets corresponding to the active ingredients screened in *Rhodiola rosea* L., the gene targets of Sal and the gene targets for the treatment of liver cancer were all introduced into Cytoscape 3.9.1, so as to construct a network model of "traditional Chinese medicine-active ingredient-disease-potential target".

Network topological analysis of relevant gene targets for drug-treated diseases

The gene targets of *Rhodiola rosea* L. and Sal for the treatment of liver cancer were all uploaded to the String (https://cn.string-db.org/) database to obtain protein interaction relationships and imported into Cytoscape 3.9.1 software to draw a protein–protein interaction (PPI) network diagram.

Gene ontology (GO) processes and kyoto encyclopedia of genes and genomes (KEGG) pathways enrichment analysis

The acquired key targets were imported into the DAVID 11.5 database (https://david.ncifcrf.gov/home.jsp) and the species were set to homo sapiens for the enrichment analysis of GO biological processes and KEGG pathways. Subsequently, the obtained analysis results were sorted according to the number of enriched targets, and only the top data were saved.

Simulation validation of the binding affinity of Sal to key targets

The 3D structure of the target protein was downloaded from the RSCB PDB database (http://www.rcsb.org/), the water and impurities of the protein were removed via using PyMOL software. The 2D structure of the active components in drugs was downloaded from the PubChem database (https://PubChem.ncbi.nlm.nih.gov/), which was converted into a 3D structure through the Chem 3D software. Subsequently, the target protein and small molecule were hydrogenated by AutoDockTools 1.5.6 software, and the Grid Box was established with original ligand as the center. After the data was obtained, the AutoDock Vina was used for molecular docking, and the results were visualized by PyMoL software.

Experimental verification

Materials

Sal (purity: 99.56%), chloroquine diphosphate (CQ, purity: 99.65%) and rapamycin (Rap, purity: 99.30%) were all purchased from Selleck Co., Ltd (Houston, USA; cat. no. S239602, S415702 and S103912, respectively). DMEM and 1640 medium were all purchased from Hyclone Co., Ltd (Logan, USA). Fetal bovine serum (FBS) was purchased from Gibco Co., Ltd (Grand Island, USA). Double antibody was purchased from BasalMedia Co., Ltd (Shanghai, China). The cell counting kit-8 (CCK-8) kit, 4% fixative solution, 1% crystal violet stain solution, trypsin-EDTA solution, 1% osmium tetroxide, saturated uranyl acetate, lead citrate, Hoechst33342 staining kit, phalloidin staining kit, MDC staining kit, BCA protein

concentration detection kit and SDS-PAGE gel preparation kit were all purchased from Solarbio Co., Ltd (Beijing, China). Triton X-100 solution, cell Calcein/PI staining kit, one-step TUNEL apoptosis assay kit and one-step reactive oxygen speciesy (ROS) assay kit were all purchased from Beyotime Co., Ltd (Shanghai, China). Flow cytometry apoptosis assay kit was purchased from BD Co., Ltd (New York, USA). Three-color pre-stained protein marker was purchased from YEASEM Co., Ltd (Shanghai, China; cat. no. 20351ES72). Extra-enhanced chemiluminescence substrate kit was purchased from Biosharp Life Science Co., Ltd (Beijing, China; cat. no. BL520A). Mouse monoclonal Bax, rabbit polyclonal Bcl-2, rabbit polyclonal cleaved-Caspase-3, rabbit polyclonal cleaved-Caspase-9, mouse monoclonal Beclin-1 and HRP-conjugated affinipure goat anti-mouse IgG antibodies were both purchased from ProteinTech Group Co., Ltd (cat. no. 60267-1-Ig, 12789-1-AP, 25128-1-AP, 28794-1-AP, 1C10C4 and SA00001-1, respectively). Rabbit polyclonal p62, rabbit polyclonal β-Actin, rabbit polyclonal β-Tubulin and mouse monoclonal anti-GAPDH antibodies were both purchased from Gene Tex Co., Ltd (cat. no. GTX100685, GTX109639, GTX101279 and GTX627408, respectively). Rabbit monoclonal LC3B antibody was purchased from Abcam Co., Ltd (cat. no. ab192890). Mouse monoclonal PI3K, rabbit polyclonal phosphorylated (p)-PI3K, rabbit polyclonal Akt, rabbit polyclonal phosphorylated (p)-Akt, rabbit polyclonal mTOR and rabbit polyclonal phosphorylated (p)-mTOR antibodies were both purchased from ImmunoWay Biotechnology Co., Ltd (cat. no. YM3503, YP0765, YT0185, YP0006, YT2913 and YP0176, respectively). Peroxidase conjugated goat anti-rabbit IgG antibody was purchased from OriGene Technologies Co., Ltd (cat. no. TA130023). Twelve Balb/c male mice, 4–6 weeks of age, were purchased from the Experimental Animal Center of Gansu University of Chinese Medicine.

Cell cultivate and treatment

Both human hepatoma cell line (HepG2) and normal human hepatocyte line (THLE-2) were all derived from the Cell bank of Shanghai Institute of Biological Sciences (SIBS, Shanghai, China). HepG2 cells were cultured in 10% FBS enriched DMEM medium, THLE-2 cells were cultured in 10% FBS enriched RPMI-1640 medium. These cells were hatched at 37°C and 5% CO_2 humidified atmosphere. And cells were treated with or without Sal (5, 10, 20, 40 and 80 μM) and/or CQ (5, 10 and 20 μM) at 37°C for 24, 48 and 72 h. Moreover, cells were also treated with or without Sal (80 μM) and/or Rap (400 nM) at 37°C for 48 h.

Establishment of the animal model

Twelve 4–6 week-old male BLAL/c mice were randomly divided into placebo and treated groups. 2×106 cell/mL HepG2 cells (150ul cell suspension) were Injected subcutaneously under the axillary of all mice. Based on the results of our preliminary experiments, the treated group was given intraperitoneal injections of Sal (80 mg/kg) and/or CQ (5 mg/kg) every other day for 4 weeks, and the placebo group was given intraperitoneal PBS injections in the same manner. Tumor growth was observed once a week for 4 weeks. Each group of mice was sacrificed on day 28 after treatment, tumor tissue was isolated and placed in cryopreservation tubes, and stored in an ultra-low temperature freezer at -80℃ for subsequent experiments. All procedures were performed in accordance with the Guidelines for the Care and Use of Laboratory Animals of Gansu University of Chinese Medicine and were approved by the Animal Care and Use Committee of Gansu University of Chinese Medicine.

Cells viability assay

HepG2 and THLE-2 cells (5×10^3 cells/well) were transferred to 96-well plates and cultivated at 37°C with 5% CO_2 in a humidified environment. After 24 h, the cells were treated with different concentrations of Sal (0, 5, 10, 20, 40 and 80 μM) and/or CQ (5, 10 and 20 μM). When the processing time reached, 10 μL CCK-8 reagent was added into each well and the cells were incubated at 37°C in the dark for 1 h. And the cells viability assays were performed using a microplate reader (Bio-Rad Laboratories Co., Ltd, New York, USA; excitation wavelength, 450 nm).

Colony formation assay

HepG2 cells (500 cells/well) were inoculated in a 60 mm dishes and incubated in a humid environment of 37°C and 5% CO_2. After 24 hours, cells were dealt with different concentrations of Sal (0, 5, 10, 20, 40, and 80 μM) and/or CQ (5, 10, and 20 μM) for 48 h. When the intervened time was reached, the cells were cultured in complete medium (10% FBS + 90% DMEM) and incubated in an incubator (5% CO_2, 37°C) for 14 days. Colonies (> 50 cells) were fixed with 4% fixative solution for 15 min at 37°C, and stained with 1% crystal violet for 30 min at 37°C. The stained cells were photographed with an inverted microscope (IM, Olympus Co., Ltd, Tokyo, Japan; magnification, ×40 and ×200), and the colonies of each group were counted manually.

IM observation

HepG2 cells (80–90% growth density) were seeded in 6-well plates and incubated at 37˚C with 5% CO_2 in a humidified environment. After 24 h, the cells were treated with various concentrations of Sal (0, 20, 40 and 80 μM) for 48 h. Cells in blank group and treated cells were observed and photographed with an IM (magnification, ×100).

Transmission electron microscope (TEM) observation

The micro-structure of HepG2 cells treated with complete medium, Rap, CQ and/or Sal for 48 h was observed. Cells in blank group and treated cells were collected by centrifuge tube and washed twice with PBS. They were then fixed at room temperature with 2.5% glutaraldehyde for 90 min and 1% osmium tetroxide for 30 min. After gradient dehydration with 95% absolute ethanol, the cells were embedded, sectioned and stained with saturated uranyl acetate and lead citrate. Finally, the cells were observed and photographed with a TEM (Hitachi Co., Ltd, Tokyo, Japan; magnification, ×5,000 and ×8,000).

Phalloidin staining

HepG2 cells (80–90% growth density) were placed in 24 wellplates on a slide at 37˚C for 24 h, and then treated with different concentrations of Sal (0, 20, 40 and 80 μM) for 48 h. The slides were washed once with PBS and fixed at room temperature with 4% fixative solution for 15 min. Subsequently, the slides were washed twice with PBS, covered with 0.3% Triton X-100 solution at at 37°C for 5 min, stained with 50 μL/well phalloidin dye in the dark at 37°C for 60 min, and washed with PBS for three times. Then, the slides were stained with DAPI dye in the dark at 37°C for 5 min, and washed twice with PBS. Finally, the

stained cells were observed under a fluorescence microscope (Olympus Co., Ltd, Tokyo, Japan; excitation wavelength, 488 nm; magnification, ×200).

Hoechst33342 staining

HepG2 cells (80–90% growth density) were placed in 12 wellplates on a slide at 37˚C for 24 h, and then treated with different concentrations of Sal (0, 20, 40 and 80 μM) and/or CQ (5, 10 and 20 μM) for 48 h. The slides were washed twice with PBS and fixed at room temperature with 4% fixative solution for 15min. Subsequently, the slides were stained with 10 μg/mL Hoechst33342 dye in the dark at 37°C for 30 min, and wished twice with PBS. Finally, the stained cells were observed under a fluorescence microscope (excitation wavelength, 488 nm; magnification, x100, ×200).

Calcein/PI staining

HepG2 cells (5×10^3 cells/well) were transferred to 96-well plates and cultivated at 37°C with 5% CO_2 in a humidified environment. After 24 h, the cells were treated with different concentrations of Sal (0, 20, 40 and 80 μM) for 48 h. The cells were washed twice with PBS. Subsequently, the cells were stained with Calcein/PI dye in the dark at 37°C for 30 min. Finally, the stained cells were observed under a fluorescence microscope (excitation wavelength, 488 nm; magnification, ×200).

TUNEL staining

HepG2 cells (80–90% growth density) were placed in 24 wellplates on a slide at 37˚C for 24 h, and then treated with different concentrations of Sal (0, 20, 40 and 80 μM) for 48 h. The slides were washed once with PBS and fixed at room temperature with 4% fixative solution for 15min. Subsequently, the slides were washed twice with PBS, covered with 0.3% Triton X-100 solution at 37°C for 5 min, stained with 50 μL/well TUNEL dye in the dark at 37°C for 60 min, and washed with PBS for three times. Then, the slides were stained with DAPI dye in the dark at at 37°C for 5 min, and washed twice with PBS. Finally, the stained cells were observed under a fluorescence microscope (excitation wavelength, 550 nm; magnification, ×100).

MDC staining

HepG2 cells (80–90% growth density) were placed in 12 wellplates on a slide and incubated at 37˚C for 24 h. The blank group and treated cells were washed twice with 1x washing buffer, stained with MDC dye in the dark at 37°C for 30 min, and then washed again with 1x washing buffer twice. Finally, the stained cells were observed with a fluorescence microscope (excitation wavelength, 355 nm, magnification, ×200).

ROS staining

HepG2 cells (80–90% growth density) were placed in 24 wellplates on a slide at 37˚C for 24 h, and then treated with different concentrations of Sal (0, 20, 40 and 80 μM) for 48 h. The slides were washed once with PBS and fixed at room temperature with 4% fixative solution for 15min. Subsequently, the slides

were washed twice with PBS, stained with 50 μL/well DCFH dye in the dark at 37°C for 30 min, and washed again with PBS for three times. Finally, the stained cells were observed under a fluorescence microscope (excitation wavelength, 550 nm; magnification, ×100).

JC-1 staining

The cells (80–90% confluence) were plated in 24 wellplates on a slide at 37˚C for 24 h. Following incubation, the cells in blank group and treated cells were washed twice with PBS, stained with JC-1 staining dye (200x JC-1 dye : ultrapure water : 5x JC-1 staining buffer = 1 : 160 : 40) for 20 min at 37˚C, and washed twice with pre-cooled 1x JC-1 staining buffer. The stained cells were observed under a fluorescence microscope (excitation wavelength, 490 nm or 525 nm; magnification, ×200).).

Flow cytometry assay

HepG2 cells (80–90% growth density) were seeded in 6-well plates and incubated at 37˚C with 5% CO_2 in a humidified environment. After 24 h, the cells were treated with various concentrations of Sal (0, 20, 40 and 80 μM) for 48 h. The treated cells were digested, centrifuged and collected. An annexin V-FITC apoptosis detection kit (Invitrogen) was used for annexin V(AV) and propidium iodide (PI) staining of cells, and the percentage of apoptotic cells was determined by using flow cytometry (Bio-Rad Co., Ltd, New York, USA).

Hematoxylin and eosin (H & E) staining

The isolated tumor tissue was placed in a cryopreserved tube containing 4% tissue fixative solution in advance and fixed overnight. On the next day, the fixed tumor tissue was removed from the cryopreservation tube with forceps and performed through three steps, including sectioning, embedding, and dewaxing. Subsequently, theses sections were stained with hematoxylin for 2 min, rinsed with distilled water, treated with 0.1% hydrochloric acid and LiCO3, rinsed with tap water for 15 min, stained with eosin for 1 min, gradient alcohol dehydration, xylene transparent treatment, and neutral gel seal. Finally, the stained sections were observed and photographed with an IM (Olympus Co., Ltd, Tokyo, Japan; magnification, ×400).

Immunohistochemistry

Firstly, the embedded tumor tissue sections were dewaxed, incubated with 3% hydrogen peroxide to block endogenous peroxidase, and blocked with diluted goat serum at 37°C for 1 h to reduce non-specific staining. Then, the tumor tissue sections were incubated with the diluted primary antibody (Bax, Bcl-2, 1:200) overnight at 4°C. On the next day, the tumor tissue sections were incubated with enzyme-labeled secondary antibodies (1:500) and chromogenic agents. Subsequently, the sections were counterstained, dehydrated, and encapsulated. Finally, the stained sections were observed and photographed with an IM (magnification, ×400).

Western blotting

The HepG2 cells and tumor tissues were all lysed on ice with RIPA buffer containing 1% PMSF. The concentration of total protein was detected by a BCA protein assay. Subsequently, the proteins (30 μg/line) were putted into SDS-PAGE (6%, 10% or 15%), and moved to a PVDF membrane. The membranes were sealed with 5% skimmed milk for 2 h at room temperature and washed with Tris-buffered saline containing 0.05% Tween-20 for 15 min. Followed by incubation with primary antibodies at 4°C overnight: anti-Bax antibody (1:1,000), anti-Bcl-2 antibody (1:1,000), anti-cleaved-Casepase-3 antibody (1:1,000), anti-cleaved-Casepase-9 antibody (1:1,000), anti-Beclin-1 (1:2,000), anti-p62 antibody (1:1,000), anti- LC3B antibody (1:1,000), anti-PI3K antibody (1:1,000), anti-p-PI3K antibody (1:500), anti-Akt antibody (1:1,000), anti-p-Akt (1:500), anti-mTOR (1:1,000), anti-p-mTOR antibody (1:500), and anti-GAPDH antibody (1:5,000) or anti-*β*-Actin antibody (1:2,000) or anti-*β*-Tubulin antibody (1:2,000). The membranes were hatched with appropriate secondary antibodies (1:5,000) for 2 h at 37°C. The proteins were detected by an extra-enhanced chemiluminescence substrate kit and Gel imaging system (Bio-Rad Laboratories Co., Ltd, New York, USA). And the Image Lab 5.1.0 software (Bio-Rad Laboratories Co., Ltd, New York, USA) was used to analyse the results.

Statistical analysis

Using IBM SPSS 22.0 statistical software (SPSS Inc., Chicago, USA) to analyze the experimental data. Data were expressed as *mean ± standard deviation* (SD). It was considered that $P < 0.05$ represented statistical difference and $P < 0.01$ represented significant difference. Differences between multiple groups were compared using one-way ANOVA followed by Tukey's post hoc test. The graphs were created by GraphPad Prism 8.0. 2 software (GraphPad Software Inc., San Diego, USA).

Results

Acquisition of targets for Rhodiola rosea L and Sal in the treatment of

liver cancer

Using "*Rhodiola rosea* L" as a keyword, a total of 22 major active ingredients of *Rhodiola rosea* L. that met the conditions were obtained from the TCMSP database, BATMAN-TCM database, Herb database, ETCM database and existing literature (Table 1), and a total of 556 targets from the corresponding ingredients were also obtained. "Liver cancer", as a keyword, was entered into the GeneCards database, OMIM database and DisGeNET database to search for liver cancer targets, and a total of 19681 disease-related targets of liver cancer were obtained. After these acquired *Rhodiola rosea* L. gene targets and liver cancer gene targets were intersecyed, a total of 485 gene targets for *Rhodiola rosea* L treatment in liver cancer were obtained (Fig. 1).

Table 1 Active ingredients and ADME parameters of *Rhodiola rosea* L.

Figure 1 Venn diagram of overlapping targets between drug and disease.

Network analysis of “traditional Chinese medicine-active ingredients-disease-

potential targets”

The 22 drug ingredients and 485 drug-disease common targets were introduced into Cytoscape 3.8.0 software to construct a network map of "traditional Chinese medicine-active ingredients-liver cancer-potential targets". Through the analysis of the data, it was finally obtained that 22 active ingredients of *Rhodiola rosea* L acted on 77 common targets of liver cancer, including 100 nodes and 152 pairs of interactions, each pattern represented a node, the connection represented the connection of each node, the red "V" shaped pattern represented *Rhodiola rosea* L, the green circular pattern represented the active ingredient of *Rhodiola rosea* L (including Sal), and the blue node pattern indicated the target of *Rhodiola rosea* L in the treatment of liver cancer (Fig. 2A). The results were analyzed using a network analyzer and indicated mean values of the network degree, betweenness centrality, and closeness centrality of 3.04, 169.64, and 40.50, respectively. The top active ingredients were the quercetin, Sal, geraniol, lemongrass acid, tricin, kaempferol, phytol, n-cetane, p-coumaric acid, salipurposide, o-cresol, n-octanol, myrcene, linalool, citral, borneol, umbelliferone, kaempferol-8-rhamnoside, kaempferol-10-rhamnoside, gallic acid, ethyl gallate, and 1-decanol. According to the results of topological parameters (Table 2), Sal has more potent activity, and therefore, has been the subject of more pharmacological research. Moreover, it may be an important active component of *Rhodiola rosea* L in the treatment of liver cancer. Subsequently, we continued to import the common targets of Sal and liver cancer into Cytoscape 3.8.0 software, and constructed a network map of "Sal-liver cancer-potential targets". Through the analysis of the data, a total of 44 potential targets of Sal acting on liver cancer were obtained, including 45 nodes and 44 pairs of interactions, each pattern represented a node, the connection represented the connection of each node, the yellow rhombus pattern represented Sal, the red "V" pattern represented *Rhodiola rosea* L, and the purple circular pattern indicated the potential target of Sal acting on liver cancer (Fig. 2B and C).

Figure 2 Construction of a “traditional Chinese medicine-active ingredients-diseases-potential targets” network. (A and B) Construction of a “*Rhodiola rosea* L-active ingredients-liver cancer-potential targets” network. (C) Construction of a “*Rhodiola rosea* L-Sal-liver cancer-potential targets” network. Sal, salidroside.

Table 2 Topological analysis of *Rhodiola rosea* L-active ingredients-potential targets network.

PPI network analysis and key target screening results

The 485 *Rhodiola rosea* L targets for the treatment of liver cancer were all imported into the STRING 11.5 database, the PPI network was obtained, and the obtained data were imported into Cytoscape 3.9.1 to draw a PPI network diagram. As shown in Fig. 3A, the nodes in the PPI network represented proteins, and the edges represented the interactions between proteins, involving a total of 455 nodes and 7707 edges.

Notably, the nodes were distributed centripetally according to the size of the degree value, the node in the center is the largest, decreasing outward, the color of the center part was the darkest, and the outward color gradually became lighter. Subsequently, we analyzed the acquired PPI network map by using the CytoHubba algorithm tool in Cytoscape 3.9.1 software. As shown in Fig. 3B, according to the obtained Degree value, the top 20 most closely related targets were screened, including AKT1, TNF, IL6, TP53, ACTB, IL1B, EGFR, MYC, HIF1A, MMP9, ESR1, BCL2, NFKB1, CASP3, PTGS2, JUN, PPARG, HSP90AA1, IL10, and CCL2. Then, the intermediate and proximity values of candidate targets were obtained by cellular NCA plugin analysis. Targets greater than degree, intermediate and near median were screened, and 10 key targets were further identified, including AKT1, TNF, IL6, TP53, ACTB, IL1B, EGFR, MYC, HIF1A, and MMP9 (Fig. 3C). We speculated that these key targets might play a critical role in the pharmacological process involved in the treatment of liver cancer.

Figure 3 Network topological analysis between “protein-protein”. (A) PPI network of potential targets (the size and color depth of nodes are proportional to the degree value). (B) Point bar graph of degree-value points for 20 key targets. (C) Key targets screening process. Among the selected key targets, the top 10 targets with the degree value are represented by yellow. The thickness and color depth of the edge are directly proportional to the correlation between the targets. PPI, protein-protein interaction.

GO processes enrichment analysis of the common targets

The 485 key targets of *Rhodiola rosea* L for the treatment of liver cancer were all imported into the DAVID database, and the species were set as homo sapiens for enrichment analysis of GO processes. The enrichment results were taken as the top 10, and concentric circles and cylindrical enrichment charts were made for display. As shown in Fig. 4A and B, the top 10 of biological process (BP) were positive regulation of protein phosporylation, positive regulation of transcription from RNA polymerase II promoter, positive regulation of gene expression, positive regulation of transcription, DNA-templated, negative regulation of apoptotic process, positive regulation of cell proliferation, positive regulation of pri-miRNA transcription from RNA polymerase II promoter, response to xenobiotic stimulus, positive regulation of apoptotic process, and positive regulation of peptidy-serine phosphorylation, respectively. The top 10 of cellular component (CC) were macromolecular complex, extracellular region, extracellular space, nucleoplasm, chromatin, nucleus, transcription factor complex, platelet alpha granule lumen, cytosol, and cytoplasm, respectively. The top of 10 molecular function (MF) were enzyme binding, identical binding, protein binding, transcription coactivator binding, ubiquitin protein ligase binding, transcription factor activity, sequence-specific DNA binding, RNA polymerase II transcription factor activity, ligand-activated sequence-specific DNA binding, protein kinase activity, growth factor activity, and RNA polymerase II sequence-specific DNA binding transcription factor binding, respectively.

Figure 4 Enrichment analysis of the GO organisms. (A) Concentric circle plot of GO biological enrichment analysis. (B) Histogram of the GO biological enrichment analysis. GO, gene ontology.

KEGG pathways enrichment analysis of the common targets

The 485 key targets of *Rhodiola rosea* L for the treatment of liver cancer were all imported into the DAVID database, and the species were set as homo sapiens for enrichment analysis of KEGG pathways. The enrichment results were taken as the top 10, and bubble and bar charts were made for display. As shown in Fig. 5A and B, the top 10 of signaling pathways were pathways in cancer, chemical carcinogenesis-receptor activation, PI3K-AKT signaling pathway, lipid and atherosclerosis, human cytomegalovirus infection, hepatitis C, kaposi saroma-associated herpesvirus infection, human T-cell leukemia virus 1 infection, human papillomavirus infection, hepatitis B, proteoglycans in cancer, AGE-RAGE signaling pathway in diabetic complications, cellular senescence, endocrine resistance, breast cancer, hepatocellular carcinoma, epstein-barr virus infection, prostate cancer, fluid shear stress and atherosclerosis, and gastric cancer, respectively. Among them, the PI3K/AKT signaling pathway ranked third in terms of enrichment, involving a total of 24 potential targets.

Figure 5 Enrichment analysis of the KEGG pathways. (A) Bubble diagram of KEGG pathway enrichment analysis. (B) KEGG pathway classification diagram. KEGG, kyoto encyclopedia of genes and genomes.

Following the results of KEGG pathway enrichment, we focused on the PI3K/AKT signaling pathway. After being phosphorylated by upstream signals, the PI3K/AKT pathway can stimulate downstream proteins (including eNOS, mTOR, GSK3, CREB, Caspase-9, MDM2, Nrf2 and NF-κB) to induce a cascade response that is involved in alleviating inflammation, inhibiting oxidative stress, stimulating angiogenesis, and many other biological processes (Fig. 6). These biological processes are often closely related to the occurrence and development of tumors, while also implying that the PI3K/AKT signaling pathway seems to be a key pathway for effective ingredients of *Rhodiola rosea* L in the treatment of liver cancer.

Figure 6 Molecular mechanism diagram of predicting drug therapy for disease. (A and B) Predicted mechanism of potential targets of Sal for HCC treatment via the PI3K/AKT signaling pathway. Sal, salidroside; HCC, hepatocellular carcinoma.

Analysis of molecular docking and visualization results between core

targets and Sal

According to the results of modern pharmacolog, Sal is the most abundant active ingredient in root of the *Rhodiola rosea* L Notably, the PI3K/AKT signaling pathway can undergo a cascade response to mediate mitochondrial apoptosis, which affects the development of tumors. Interestingly, mTOR, is not only one of the downstream proteins of the PI3K/AKT signaling pathway, but is also closely correlated with the occurrence of autophagy. Therefore, in order to further study the intrinsic molecular mechanism of

Rhodiola rosea L in liver cancer treatment, the PI3K/AKT/mTOR signaling pathway-related targets (PI3K, AKT and mTOR), mitochondrial apoptosis-related targets (Bax, Bcl-2, Caspase-3 and Caspase-9), and autophagy-related targets (Beclin-1, p62 and LC3B) and Sal were performed respectively molecular docking by using AutoDock Vina 1.1.2 software. According to the relevant literature records, the lower the binding energy of the ligand to the receptor, the more stable the binding interaction. Binding energies less than − 5 kcal/mol indicate a good binding capacity, and less than − 7 kcal/mol indicate a strong binding capacity [19]. As shown in Fig. 7, The docking binding energy heatmap showed that all 10 groups had docking binding energies less than − 5.0 kcal/mol, and most of them had binding energies less than − 6.0 kcal/mol, with an average binding energy of − 6.39 kcal/mol. This suggested that all molecules have strong binding affinities with Sal. The combinations with stronger binding interactions were PI3K and Sal, and p62 and Sal, with − 8.0, and − 8.1 kcal/mol, respectively, indicating that these active components have strong binding affinity for their targets and may play an important role in the treatment of liver cancer by Sal.

Figure 7 Molecular docking binding energy heatmap (the color shade is inversely proportional to the magnitude of the binding energy).

Furthermore, we visualized the docking results of 10 small molecules with Sal. As shown in Fig. 8, these small molecules were all bound in a deep cavity inside the receptor protein, and they had good shape complementarity. Notably, theses binding sites were both hydrophobic and hydrophilic, involving various modes of interaction, such as hydrogen bonding, vander waals forces, carbon–hydrogen bonding, and π–π stacking. In the docking of molecular targets associated with signaling pathways, Sal was interacted with amino acid residues on the active site of PI3K, including TYR496, GLN645, VAL672, LEU648, PRO669, MET394, and LEU393. Sal was interacted with amino acid residues on the active site of AKT, including GLU85, LYS20, GLY16 and ARG15. Sal was interacted with amino acid residues on the active site of mTOR, including GLU2084, GLN2083 and MET2059 (Fig. 8A). In the docking of molecular targets associated with mitochondrial apoptosis, Sal was interacted with amino acid residues on the active site of Bax, including SER126, LY8123, GLN77 and LYS119. Sal was interacted with amino acid residues on the active site of Bcl-2, including GLY193, ASN182, ASN11, ASP10, GLY8 and TYR9. Sal was interacted with amino acid residues on the active site of Caspase-3, including GLN161, CYS163, HIS121, MET61, SER120 and ARG64. Sal was interacted with amino acid residues on the active site of Caspase-9, including GLU351, TRP348, ASP342 and SER345 (Fig. 8B). Moreover, In the docking of molecular targets associated with autophagy, Sal was interacted with amino acid residues on the active site of Beclin-1, including TYR328 and VAL370. Sal was interacted with amino acid residues on the active site of p62, including ASP69, CYS44 and ASP80. Sal was interacted with amino acid residues on the active site of LC3B, including LEU47, VAL46, ARG37 and LYS39 (Fig. 8C).

Figure 8 Molecular docking analysis of Sal to key targets. (A) Signaling pathway-related targets (including PI3K, AKT and mTOR)–Sal interaction surface and 2D and 3D images of the molecular docking results. (B) Mitochondrial apoptosis-related targets (including Bax, Bcl-2, Caspase-3 and Caspase-9)–Sal interaction surface and 2D and 3D images of the molecular docking results. (C)

Autophagy-related targets (including Beclin-1, p62 and LC3B)–Sal interaction surface and 2D and 3D images of the molecular docking results. Sal, salidroside.

Sal suppressed viability and proliferation of HepG2 cells in vitro

HepG2 cells were respectively dealt with various concentrations (5, 10, 20, 40 and 80 μM) of Sal for 24, 48 and 72 h. As presented in Fig. 9A, compared with the blank group, Sal had both inhibitory effects on the viability of HepG2 cells with dose-dependent manner at different times ($P < 0.05$). Moreover, the values of half maximal inhibitory concentration (IC_{50}) at 24, 48 and 72 h were 70.9, 30.5 and 17.9 μM (Fig. 9B). To evaluate the safety of Sal, human liver normal cells THLE-2 were also dealt with various concentrations (5, 10, 20, 40 and 80 μM) of Sal for 48 h. As presented in Fig. 9C, the results demonstrated that Sal had no significant change on the viability of THLE-2 cells ($P > 0.05$). Based on the results of above experiments, we mainly chose to treat HepG2 cells with Sal (20, 40, 80 μM) for 48 h as the processing conditions into subsequent experiments. Meanwhile, following treatment with Sal (20, 40 and 80 μM) for 48 h, the count of colonies (> 50 cells) indicated that the Sal group inhibited the proliferative capacity of HepG2 cells with a dose-dependent manner, compared with those in the blank group (Fig. 9D).

Figure 9 Sal-suppressed viability and proliferation in HepG2 cells. (A) The effects of Sal at various concentrations on the proliferation in HepG2 cells by CCK-8 method. $^{*}P < 0.05$, $^{**}P < 0.01$ vs. blank. (B) The results of IC_{50} in Sal-treated HepG2 cells by CCK-8 method. (C) The toxicological effects of Sal on human liver normal cells THLE-2 by CCK-8 method. $^{**}P < 0.01$ vs. blank. (D) The effects of Sal on the proliferative ability in HepG2 cells were observed by the plate colony formation experiment. Magnification, x40, x200. Sal, salidroside; IC_{50}, half maximal inhibitory concentration.

Sal induced the process of apoptosis in HepG2 cells

Apoptosis has unique morphological characteristics and energy-dependent biochemical mechanism. Cell pyknosis, cell contraction and chromatin condensation usually occur in the early stage of apoptosis [20, 21]. The post-apoptotic germination of cells is the result of the formation of apoptotic bodies containing closely arranged organelles by a large number of plasma membrane vesicles [22]. In this study, we treated the HepG2 cells for 48 h with different concentrations of Sal. After Sal intervention, the results of IM observation showed that the number of apoptosis after Sal treatment increased dose-dependently compared with the blank group, and the intercellular space was gradually widened (Fig. 10A). In order to better observe the effect of Sal on cell morphology, the phalloidin staining was used to visualize the cytoskeleton of each group. As shown in Fig. 10B, untreated cells were mostly long spindle-shaped, and the nuclei were located in the cytoskeleton. However, the Sal treated cells underwent skeleton shrinkage and deformation, nuclear chromatin condensation, nuclear exomigration, nuclear shrinkage rupture and so on. Moreover, the results of Hoechst33342 staining, Calcein/PI staining and TUNEL staining also showed that the Sal treated group increased the number of apoptosis in a dose-dependent manner compared to the blank group (Fig. 10C-E).

Figure 10 Sal-induced apoptosis in HepG2 cells. (A and B) The cellular morphology after Sal treated was observed by using IM and phalloidin staining. Magnification, ×100. (C, D and E) The phenomenon of apoptosis after Sal treated was observed by using Hoechst33342 staining, Calcein/PI staining and TUNEL staining. Magnification, ×100. Sal, salidroside; IM, inverted microscope.

The experimental results from flow cytometry showed that the Sal-treated group increased the total apoptosis rate in a dose-dependent manner as compared to the blank group ($P < 0.01$; Fig. 11A). To further verify the role of Sal in inducing apoptosis, the expression levels of apoptosis-related proteins in mitochondria were detected by western blot (Fig. 11B). The results showed that compared with the blank group, the ratio of Bax to Bcl-2 protein was increased, while the expression level of cleaved-Caspase-3 and cleaved-Caspase-9 proteins were also increased with a dose-dependent manner on the 2nd day after Sal treatment ($P < 0.05$).

Figure 11 Sal-induced mitochondrial apoptosis in HepG2 cells. (A) The total apoptotic rate after Sal treated was detected by using the flow cytometry. $^{*}P < 0.05$, $^{**}P < 0.01$ vs. blank. (B) The expression levels of Bax, Bcl-2, cleaved-Caspase-3 and cleaved-Caspase-9 proteins were analyzed by western blotting in HepG2 cells of each group. $^{*}P < 0.05$, $^{**}P < 0.01$ vs. blank. Sal, salidroside.

Sal induced organelle impairment and autophagosome generation

The ultrastructure of HepG2 cells treated with Sal or autophagic inducer (Rap) was observed by TEM. Compared with untreated cells (Fig. 12A), a large number of autophagosomes composing of double membranes were observed in HepG2 cells treated with Sal or Rap for 48 h (Fig. 12B and C, respectively). Cytoplasmic material and/or membrane vesicles were enclosed in autophagosomes. In addition, endoplasmic reticulum swelling and mitochondrial damage were observed after Sal or Rap treatment (Fig. 12B and C). To further verify the phenomenon of autophagy, MDC staining were used to observe the autophagy product (autophagosomes) following Sal or Rap treatment in HepG2 cells. As presented in Fig. 12D, the green fluorescence associated with autophagosomes was not found in the blank group, while green fluorescence was found in the Sal group, and the results were consistent with the 400 nM Rap group. Meanwhile, western blot analysis showed (Fig. 12E) that compared with the blank group, the ratio of LC3B-II to LC3B-I protein and the expression level of Beclin-1 protein in the Sal group were up-regulated with a dose-dependent manner ($P < 0.05$), while the expression level of p62 protein in the Sal group were down-regulated with a dose-dependent manner ($P < 0.05$).

Figure 12 Sal-induced autophagy in HepG2 cells. (A) Untreated HepG2 cells were obtained by TEM. The structures of endoplasmic reticulum and mitochondria were normal in blank group. (B and C) Swollen endoplasmic reticulum and mitochondria were appeared in Rap or Sal treatment group. In addition, autophagosomes in the cytoplasm were also appeared in Rap or Sal treatment group. Red, blue and green arrowheads respectively indicate the endoplasmic reticulum, mitochondria and autophagosomes. Magnification, ×3,000, ×8,000. (D) The green fluorescence related to autophagosomes was increased with a dose-dependent manner in Sal or Rap treatment group by using MDC staining, compared with those in

blank group. Magnification, ×200. (E) The expression levels of Beclin-1, p62, LC3B-I and LC3B-II proteins were analyzed by western blotting in HepG2 cells of each group. $^{*}P < 0.05$, $^{**}P < 0.01$ vs. blank. TEM, transmission electron microscope; Sal, salidroside; Rap, rapamycin.

Inhibiting autophagy increased mitochondrial damage

The mechanism of CQ is mainly to inhibit autophagy by preventing the combination of autophagosomes and lysosomes. Therefore, in the present study, CQ was used as a tool drug to inhibit autophagy. As presented in Fig. 13A, compared with the blank and Sal groups, the amount and brightness of green fluorescence was decreased with a dose-dependent manner in the Sal + CQ group. Moreover, the expression level of p62 protein was significantly up-modulated, while the expressions of Beclin-1 and LC3B-II/LC3B-I proteins were significantly down-modulated on days 2 after treatment with CQ ($P < 0.01$; Fig. 13B). At the same time, the expression level of Beclin-1 protein was significantly up-modulated, and the expression level of p62 protein was significantly down-modulated on days 2 after treatment with autophagy inducer Rap ($P < 0.01$; Fig. 13C). This data suggested that the CQ was effectively inhibited Sal-induced autophagy in our study.

Figure 13 CQ inhibited the Sal-induced autophagy in HePG2 cells. (A) The green fluorescence related to autophagosomes was decreased with a dose-dependent manner in the Sal + CQ group by using MDC staining, compared with the blank and Sal groups. Magnification, ×200. (B and C) The expressions of Beclin-1, p62, LC3B-I and LC3B-II proteins were analyzed by western blotting in HepG2 cells of each group. $^{**}P < 0.01$ vs. blank. $^{\#\#}P < 0.01$ vs. Sal group. Sal, salidroside; CQ, chloroquine diphosphate; Rap, rapamycin.

Mitochondria have double membrane structure, which is the key organelle to produce energy [23]. In addition, mitochondria regulate redox signaling pathway and programmed cell death [23]. In order to study the role of CQ in Sal-treated mitochondria, the micro-structure of mitochondria was observed by TEM. As presented in Fig. 14A and B, mitochondrial swelling was observed on the 2nd day after Sal treatment, compared with the blank group. And more mitochondrial damages were obviously appeared in the Sal + CQ group (Fig. 14C), consisting of serious mitochondrial swelling, double membrane destruction and loss of normal morphology, implying that inhibition of autophagy increased the degree of mitochondrial damage in Sal-treated cells.

Figure 14 Inhibiting autophagy increased mitochondrial damage in HepG2 cells. The micro-structure of mitochondria in each group were observed by TEM: (A) The morphology of mitochondria was normal in blank group. (B) The mitochondrial swellings were observed following Sal treatment for 48 h in HepG2 cells. (C) After cells were treated with Sal and CQ for 48 h, increased damage to mitochondrial morphology was observed compared with those in blank and Sal groups. Magnification, ×3,000, ×8,000. TEM, transmission electron microscope; Sal, salidroside; CQ, chloroquine diphosphate.

To verify the effect of Sal on mitochondrial function, the ROS staining, JC-1 staining and flow cytometry were added in subsequent experiments. The results were shown in Fig. 15A, where green fluorescence

represented ROS content and the ROS content was increased in 80 μM treated HepG2 cells compared to the blank group. Meanwhile, the mitochondrial membrane potential was subsequently decreased in HepG 2 cells treated with 80 μM ($P < 0.05$;Fig. 15B and C).

Figure 15 Inhibition of autophagy promoted the degree of mitochondrial dysfunction in HepG2 cells. (A) The content of ROS after Sal and/or CQ treated was observed by using ROS staining. Magnification, ×100. (B) The changes in mitochondrial membrane potential after Sal and/or CQ treated were observed by using JC-1 staining. Magnification, ×200.

CQ enhanced Sal-mediated biological processes in HepG2 cells

As previously mentioned that Sal could induce apoptosis of HepG2 cells and inhibit autophagy to accelerate the degree of mitochondrial damage in Sal-treated cells. In order to further study the role of CQ on HepG2 cells treated with Sal, CCK-8 method, plate colony formation experiment and Hochest33342 staining were used to observe the biological effect of HepG2 cells. The results of CCK-8 assay showed that compared with the blank group, 80 μM Sal group both could inhibit the viability of HepG2 cells at different times ($P < 0.01$). Besides, compared with the Sal group, the inhibitory effects on viability of HepG2 cells was all increased obviously with a dose-dependent manner in the Sal + CQ groups at different times ($P < 0.01$; Fig. 16A). Meanwhile, the results of plate colony formation experiment demonstrated that the number of colonies (> 50 HepG2 cells) was decreased at 48 h after treatment with 80 μM Sal, whereas the fewer colonies were observed in the Sal + CQ groups at 48 h after treatment, compared with those in blank group (Fig. 16B). Notably, the results of Hoechest33342 staining showed that compared with the blank group, the number of apoptotic cells following treatment with Sal for 48 h was increased, whereas the more apoptotic cells were observed in Sal + CQ group at 48 h after treatment ($P < 0.01$; Fig. 16C). To make the results more convincing, the flow cytometry was added to the subsequent experiments to calculate the total apoptosis rate in each group. As shown in Fig. 16D, the overall apoptosis rate was increase in the 80 μM Sal treated group compared with the blank group. However, the total apoptosis rate was significantly enhanced in the Sal + CQ group compared with the 80 μM Sal group ($P < 0.01$).

Figure 16 Inhibiting autophagy could improve Sal-induced apoptosis in HepG2 cells. (A) The effects of Sal combined with CQ on the growth viability in HepG2 cells were detected by CCK-8 method. $^{**}P < 0.01$ vs. blank. $^{\#\#}P < 0.01$ vs. Sal group. (B) The effects of Sal combined with CQ on the proliferative capacity in HepG2 cells were observed by the plate colony formation experiment. Magnification, ×40, ×200. (C) Apoptosis was measured by Hoechst33342 staining in HepG2 cells. Compared with the blank and Sal groups, the number of apoptotic cells were obviously increased with a dose-dependent manner in the Sal + CQ group. Magnification, ×100. (D) The total apoptotic rate after Sal combined with CQ was detected by using the flow cytometry. $^{**}P < 0.01$ vs. blank. $^{\#\#}P < 0.01$ vs. Sal group. Sal, salidroside; CQ, chloroquine diphosphate.

To sum up, these results suggested that inhibition of autophagy greatly accelerated the biological processes, consisting of promoting apoptosis, inhibiting viability and suppressed proliferation.

CQ combined Sal up-regulated the expression level of Caspase family in HepG2 cells

Autophagy and apoptosis are two important processes of catabolism [24], and the relationship between them is still unclear. In order to explore the complex cross-interference between autophagy and apoptosis, the expression of several proteins related to these processes was studied. As presented in Fig. 17A and B, the expression levels of cleaved-Caspase-3, cleaved-Caspase-9 and Bax/Bcl-2 all exhibited increasing trend in the Sal group compared with those in blank group ($P < 0.01$). Interestingly, the expression levels of cleaved-Caspase-3, cleaved-Caspase-9 and Bax/Bcl-2 after combined treatment with CQ were significantly higher than those in blank and Sal groups ($P < 0.05$). These results suggested that inhibiting autophagy might accelerate the apoptosis of HepG2 cells, mainly through the internal pathway mediated by Caspase cascade reactions.

Figure 17 Inhibiting autophagy regulated the expression levels of proteins related to apoptosis in HepG2 cells. (A) The expression levels of Bax, Bcl-2, cleaved-Caspase-3 and cleaved-Caspase-9 proteins were analyzed by western blotting in HepG2 cells of each group. (B) Quantification of Bax, Bcl-2, cleaved-Caspase-3 and cleaved-Caspase-9 proteins by the densitometry. $^{**}P < 0.01$ vs. blank. $^{\#}P < 0.05$, $^{\#\#}P < 0.01$ vs. Sal group. Sal, salidroside; CQ, chloroquine diphosphate.

CQ combined Sal inhibited tumor formation in mice

In order to make the results more convincing, the tumor xenograft trial was used to observe the effect of CQ in combination with Sal on tumor growth in mice. Firstly, H&E staining was used to observe the pathological changes of tumor tissues. The results were shown in Fig. 18A, where tumor cells in the placebo group were irregularly arranged and tightly aligned, accompanied by tumor cellular atypia. However, compared with the placebo group, although the tumor cells in the treated groups were also arranged irregularly, they were looser overall, and the number of tumor cells were also reduced. Notably, the arrangement of tumor cells in the Sal + CQ group was more loose than in the Sal-treated group, and the number of tumor cells was further reduced. Subsequently, to further validate our hypothesis, changes in the expression of tumor-associated apoptotic proteins were detected by immunohistochemistry and western Blot techniques. The results of immunohistochemistry were shown in Fig. 18B, and the expression of Bax protein in the CQ-treated group, Sal-treated group and Sal + CQ combination group was all up-regulated compared with the placebo group. Moreover, the expression of Bax protein in the Sal + CQ group was more significantly higher than that in the Sal-treated group. In contrast, the Bcl-2 protein in the placebo group had the characteristics of high expression, while the expression of Bcl-2 protein in the treated groups was relatively reduced, and the expression of Bcl-2 protein in the Sal + CQ group was more significantly lower than that in the Sal-treated group. Interestingly, the results of western blot were consistent with those of immunohistochemistry. As shown in Fig. 18C, compared to the placebo group, the expression level of Bax protein was increased in the Sal-treated group ($P < 0.01$), while the expression

level of Bcl-2 in the Sal-treated group was reduced ($P < 0.01$). Compared with Sal-treated group, CQ combined with Sal was able to further increase the ratio of Bax to Bcl-2 protein ($P < 0.01$). These findings suggested that Sal + CQ could significantly affect the expression level of apoptosis-related proteins, thereby disrupting the biological function of mitochondria and inhibiting the growth of tumor cells.

Figure 18 Sal combined with CQ could effectively inhibited tumor formation in mice. (A) The pathological changes of tumor tissues were observed by using H E staining. Magnification, ×400. (B) The expression change of Bax and Bcl-2 proteins were observed by using immunohistochemistry. Magnification, ×400. (C) The expression levels of Bax and Bcl-2 proteins were analyzed by western blotting in tumor tissues of each group. $^{*}P < 0.05$, $^{**}P < 0.01$ vs. Placebo group. $^{\#\#}P < 0.01$ vs. Sal group. Sal, salidroside; CQ, chloroquine diphosphate; H E, hematoxylin and eosin.

Sal and CQ modulated PI3K/AKT/mTOR signaling pathway

As presented in Fig. 19A and B, western blot analysis showed that the ratios of p-PI3K/PI3K, p-AKT/AKT and p-mTOR/mTOR proteins in Sal group were decreased with a dose-dependent manner compared with those in the blank group ($P < 0.01$). Interestingly, activation of PI3K/AKT/mTOR signaling pathway in Sal + CQ group was promoted with a dose-dependent manner after combining with CQ treatment compared with those in blank group and Sal group ($P < 0.05$; Fig. 19C and D). These results suggested that Sal could induce autophagy by inhibiting the activation of PI3K/AKT/mTOR signaling pathway. In other words, inhibition of autophagy might accelerate apoptosis, which was mainly associated with the activation of PI3K/AKT/mTOR signaling pathway in HepG2 cells.

Figure 19 Expression levels of proteins associated with PI3K/AKT/mTOR signaling pathway in HepG2 cells were detected by western blot. (A) The expressions of PI3K, p-PI3K, AKT, p-AKT, mTOR and p-mTOR proteins were analyzed by western blotting in HepG2 cells induced by Sal or Rap. (B) Quantification of PI3K, p-PI3K, AKT, p-AKT, mTOR and p-mTOR proteins by the densitometry. $^{**}P < 0.01$ vs. blank. (C) The expressions of PI3K, p-PI3K, AKT, p-AKT, mTOR and p-mTOR proteins were analyzed by western blotting in HepG2 cells induced by Sal and treated with CQ. (D) Quantification of PI3K, p-PI3K, AKT, p-AKT, mTOR and p-mTOR proteins by the densitometry. $^{**}P < 0.01$ vs. blank. $^{\#}P < 0.05$, $^{\#\#}P < 0.01$ vs. Sal group. Sal, salidroside; CQ, chloroquine diphosphate.

Discussion

Network pharmacology and bioinformatics have been widely used to excavate therapeutic targets for various diseases to help researchers identify differently expressed genes and potentially different signaling pathways. Network pharmacology includes virtual computing, high-throughput data analysis, and network database retrieval, involving bioinformatic network construction and network topology analysis [25]. This approach focuses on the synergy of multi-component, multi-channel and multi-target [26, 27]. Following with the recent fusion of bioinformatics, computational prediction-based network pharmacology has emerged as a powerful approach to systematically reveal the biological mechanisms

of complex diseases and drug effects at the molecular level [28, 29]. Thus, to explore the relationship between liver cancer and autophagy under the intervention of traditional Chinese medicine, we adopted a systematic method based on bioinformatics analysis, network pharmacology, and experimental verification with the combined treatment of Sal and CQ intervention on liver cancer. In this study, 22 active ingredients of *Rhodiola rosea* L, 556 related targets corresponding to components and 19,681 liver cancer-related targets were obtained from public databases. Integrating the potential targets of the above components with the potential targets of the disease, exactly 485 therapeutic targets were revealed. Based on the topological analysis of PPI networks, we selected the top 10 core targets, including AKT1, TNF, IL6, TP53, ACTB, IL1B, EGFR, MYC, HIF1A, MMP9, and speculated that these key targets might play a key role in the pharmacological process involved in the treatment of liver cancer. Subsequently, the enrichment analytic results of GO processes based on these common targets for drug-disease showed that the role of the active ingredient contained in *Rhodiola rosea* L in liver cancer is implicated in many biological processes, including positive regulation of protein phosporylation, positive regulation of transcription from RNA polymerase II promoter, positive regulation of gene expression, positive regulation of transcription, DNA-templated, negative regulation of apoptotic process, positive regulation of cell proliferation, positive regulation of pri-miRNA transcription from RNA polymerase II promoter, response to xenobiotic stimulus, positive regulation of apoptotic process, positive regulation of peptidy-serine phosphorylation, and so on. Furthermore, many related pathways were retrieved from these shared targets by the KEGG pathways enrichment technique, such as pathways in cancer, chemical carcinogenesis-receptor activation, PI3K-Akt signaling pathway, lipid and atherosclerosis, human cytomegalovirus infection, hepatitis C, kaposi saroma-associated herpesvirus infection, human T-cell leukemia virus 1 infection, human papillomavirus infection, hepatitis B, proteoglycans in cancer, AGE-RAGE signaling pathway in diabetic complications, cellular senescence, endocrine resistance, breast cancer, hepatocellular carcinoma, epstein-barr virus infection, prostate cancer, fluid shear stress and atherosclerosis, gastric cancer and so on. Apparently, *Rhodiola rosea* L can treat liver cancer via the PI3K/Akt signaling pathway. The PI3K/Akt signaling pathway can mediate mitochondrial apoptosis through cascade reactions, so as to affect the occurrence and development of tumors. Interestingly, mTOR is not only one of the downstream proteins of the PI3K/AKT signaling pathway, but is also closely related to the occurrence of autophagy. Notably, according to the topological parameter results of 22 active ingredients from *Rhodiola rosea* L and combining with existing pharmacological studies, Sal has stronger biological activity among these 22 ingredients, so it is favored by many researchers. Moreover, it may also be an important active ingredient of *Rhodiola rosea* L in the treatment of liver cancer. Therefore, in order to further study the intrinsic molecular mechanism of *Rhodiola rosea* L in the treatment of liver cancer, we selected PI3K/Akt/mTOR signaling pathway-related targets (PI3K, AKT and mTOR), mitochondrial apoptosis-related targets (Bax, Bcl-2, Caspase-3 and Caspase-9), and autophagy-related targets (Beclin-1, p62 and LC3B) to be intersected with Sal. The results showed that these key targets showed good binding ability with Sal, suggesting that Sal might adjust autophagy flux based on PI3K/Akt/mTOR signaling pathway, thereby affecting the occurrence and development of liver cancer.

Subsequently, based on the analysis results of network pharmacology, we investigated the role of Sal in HCC through cell experiments, focusing on the autophagy pathway. Autophagy is actually a “self-eating” phenomenon in cells. When cells are received some stimuli (such as starvation or hypoxia), the mechanism of autophagy is activated. Senescent or damaged organelles are wrapped by the double-layered membrane of autophagic vesicles to constitute autophagosomes, which are combined with lysosomes to constitute autolysosomes. Autolysosomes can degrade the wrapped substances by its hydrolase, and the degraded products can be used to preserve the stability of internal environment and renewal of organelles [9]. Thus, the morphological features of autophagy are characterized by the construction of autophagic vesicles and accumulation of acidic organelles (autophagosomes and autolysosomes) [30]. More and more data have shown that the occurrence of autophagy is associated with certain proteins, which are called autophagy-related proteins. Beclin-1, p62 and LC3B have been confirmed to be key proteins in autophagy. The Beclin-1 gene, which encodes the autophagy-induced protein, mainly modulates the localization of other autophagy-related proteins in the structure of autophagy precursors by forming a complex with type III PI3K, so as to regulate the activity of autophagy [31, 32]. The p62 protein can bind with LC3, which lies in the membrane of autophagic vesicle, so as to recruit the autophagic degradation substrate into the autophagic vesicle for completing the process of degradation [33, 34]. Autophagy-related molecules (such as Atg3 and Atg7) can modify LC3-I through a ubiquitin lipid-like coupling system, the modified LC3-I can be covalently inserted as the form of phosphatidylethanolamine (PtdEth, PE) into the autophagosome, so as to convert into LC3-II, and the transform of LC3-I to LC3-II further promotes the formation of autophagosomes [35].

Apoptosis is an active physiological reaction and the main form of type I programmed cell death, which is identified by eversion of membrane, condensation of nuclear chromatin, split of nucleus, formation of apoptotic bodies and so on [8]. Apoptosis is triggered via various signaling pathways, consisting of the extrinsic and intrinsic signaling pathway [36]. Among them, intrinsic signaling pathway mainly occurs in mitochondria. When cells are stimulated by some signals of death (such as cell hypoxia, lack of cell growth factors), the pathway of mitochondrial apoptosis is activated to cause cell apoptosis [37]. A large number of evidences have indicated that some proteins can induce apoptosis via the pathway of mitochondrial, including Bax, Bcl-2, Caspase-3, Caspase-9 proteins and so on [38, 39]. Bax is known as a protein of pro-apoptosis, and Bcl-2 is known as a protein of anti-apoptosis. The ratio of Bax to Bcl-2 can alter the potential of mitochondrial membrane, so as to release cytochrome C, which combines with Apaf-1 to trigger the cascade reaction of Caspase family. Caspase-3 has been confirmed to be downstream of this cascade reaction. It causes cell death by degrading corresponding intracellular substrates. Caspase-9, as a downstream member of Caspase-3, can damage the nuclear pore in certain ways, help caspase-3 enter the nucleus and hydrolyze deoxyribonuclease inhibitor (ICAD). The ICAD is hydrolyzed and separated by caspase-3 to release CAD, so as to cause DNA degradation, cytoskeleton separation, nuclear fragmentation, and so on [40]. Thus, “Caspase” family, especially Caspase-3 and Caspase9, plays a dominant effect in the intrinsic pathway of apoptosis.

Stimulating cell stress (such as hypoxia and starvation) can make cells play a dual role [41]. Cells can activate cytoprotective pathways, such as autophagy, to maintain the stability of the intracellular

environment until the stress is eliminated. On the contrary, cells can also undergo programmed cell, such as apoptosis. More and more studies have suggested that autophagy and apoptosis may play a pivotal role in cancer. In the process of tumorigenesis and development, autophagy may play two opposite roles: on the one hand, autophagy acts as a protective mechanism to resist stress response and inhibit apoptosis. For example, Wang *et al.* [10] have confirmed that pseudolaric acid B can induce autophagy and inhibit apoptosis in human lung fibroblasts MRC5 cells through the response of DNA damage. In addition, autophagy can also produce some products (such as fatty acids, amino acids and so on), which provide nutrients for the growth of tumor [11, 12]. On the other hand, autophagy can synergistically induce apoptosis. For example, resveratrol can synergistically treat ovarian cancer by inducing autophagy in human ovarian cancer cells [13]. The combined treatment of matrine and 5-fluorouracil can up-regulate the expression of autophagy-related genes Atg5 and Beclin-1 to enhance its chemosensitivity [14]. Thus, these studies are suggested that there is a complex interaction between autophagy and apoptosis. Studying the potential interaction mechanism under different cellular stress environment will help to understand the relationship between autophagy and apoptosis.

Cellular stresses stimuli can also be occurred in a long-term drug intervening environment, so as to induce autophagy and/or apoptosis. More and more studies have shown that glycosides, which are derived from traditional Chinese medicine, can also treat cancer through the pathway of autophagy. For example, ginsenoside F2 induces autophagy by up-regulating the expressions of Atg7, Beclin1, and LC3B proteins in human breast cancer stem cells, while activating the pathway of mitochondrial apoptosis, and the combined treatment of autophagy inhibitor chloroquine can enhance the ginsenoside F2-induced apoptosis [15]. The results of the present study were consistent with this finding: On the one hand, we found that Sal had inhibitory effect on the growth of HepG2 cells by CCK-8 method and plate colony formation assay. Then, we also observed that Sal could effect the shape of HepG2 cells (including the cytoskeleton was wrinkled and rounded, the nucleus was transferred outward and so on) by IM and phalloidin staining. Moreover, we found that Sal could damage the shape of mitochondria in HepG2 cells by TEM, promote the release amount of ROS by corresponding assay kit and increase the number of apoptotic cells by various staining methods (including Hoechst33342 staining, Calcein/PI staining and TUNEL staining), while up-regulate the expression levels of Bax/Bcl-2, cleaved-Caspase-3 and cleaved-Caspase-9. One the other hand, we observed that Sal could induce HepG2 cells to produce some ultrastructures (such as autophagic vesicles, autophagosomes and autolysosomes) by TEM and MDC staining. Then, we also found that Sal induced autophagy by up-regulating the expression of Beclin-1 and LC3-II/I proteins, down-regulating the expression of p62 protein in HepG2 cells. Thus, the data suggested that Sal induced autophagy, while activating the pathway of mitochondrial apoptosis. Notably, after CQ inhibited autophagy, mitochondrial damage and dysfunction were increased, which is accompanied by an increase in the level of ROS. In addition, after inhibition of autophagy, the expression levels of apoptosis-related proteins were increased obviously, consisting of Bax/Bcl-2, cleaved-Caspase-3 and cleaved-Caspase-9. Meanwhile, the number of apoptotic cells was also increased significantly. Interestingly, through in vivo experiments, we also verified that CQ combined with Sal could effectively inhibit the growth of tumor cells (HepG2). To sum up, the current results indicated that CQ treatment

mainly promoted Sal-induced apoptosis of HepG2 cells through Caspase-9-dependent intrinsic apoptotic pathway. In addition, these results suggested that autophagy might play a protective role in the early stage of liver cancer injury in the Sal-treated environment.

There is more and more evidence of cross-interference between autophagy and apoptosis, because they both have some regulatory molecules, such as Bcl-2 and PI3K/AKT/mTOR signaling pathway. PI3K/AKT signaling pathway is a classical pathway to regulate apoptosis. This pathway affects the status of downstream apoptosis-related molecules (Bax, Bcl-2, Caspase-3, Caspase-9) in various ways, so as to regulate the proliferation and apoptosis of cancer cells [42, 43]. For example, Chen *et al.* [44] treated human gastric cancer SGC7901 cells with quercetin, which were extracted from Dendrobium bark, and they found that quercetin decreased the expression levels of p-PI3K and p-AKT proteins, and up-regulated the expression level of Caspase-3 protein, suggesting that quercetin might induce apoptosis of SGC7901 cells by inhibiting PI3K/AKT signaling pathway. Similar to their results, our data showed that Sal decreased the phosphorylation of PI3K and AKT proteins, while up-regulate the expression levels of Bax/Bcl-2, cleaved-Caspase-3 and cleaved-Caspase-9 proteins. mTOR is not only the downlink target of PI3K/AKT pathway, but also plays an important role in regulating autophagy [45, 46]. For example, Rong *et al.* [47] used Sal to deal with human gastric cancer AGS cells in vitro, and they found that Sal decreased the expression levels of p-PI3K, p-AKT and p-mTOR proteins, while Sal combined with autophagy inhibitor (IGF-1) decreased the expression levels of Beclin-1 and LC3-II proteins, indicating that Sal induced autophagy of AGS cells through PI3K/AKT/mTOR signaling pathway. Similar to their results, our data showed that Sal decreased the phosphorylation of PI3K, AKT and mTOR proteins, and the combined treatment of Sal and CQ increased the expression levels of p-PI3K, p-AKT and p-mTOR proteins. Meanwhile, Sal up-regulated the expression levels of Beclin-1 and LC3-II/LC3-I proteins, while down-regulated the expression level of p62 protein. It is suggested that Sal may trigger a series of autophagy and mitochondrial apoptosis of HepG2 cells by inhibiting PI3K/AKT/mTOR signaling pathway. Furthermore, the signaling pathway was activated following autophagy inhibition with CQ, so as to accelerate the apoptotic process. It is suggested that PI3K/AKT/mTOR signaling pathway may play an important role in regulating the crosstalk between autophagy and apoptosis.

Conclusion

In summary, the characteristics of “multi-target and multi-channel” of Sal in the treatment of HCC were systematically analyzed by network pharmacodynamic method, in vitro and in vivo experiments. Notably, our in vitro and vivo validation unexpectedly corresponds with the predictions of the network pharmacological analysis. Our study confirmed that Sal showed anticancer activity in vitro and vivo, and inhibited the proliferation of human hepatoma cells. Meanwhile, a series of experiments verified that Sal induced apoptosis and autophagy through targeting PI3K/AKT/mTOR signaling pathway. Moreover, Sal-induced autophagy was a mechanism to protect human hepatoma cells from external attacks. Excitingly, our data suggested that autophagy inhibitors (CQ) could promote Sal-induced apoptosis of human hepatoma cells (Fig. 20). In other words, our study not only provided theoretical and experimental basis for the anti-HCC activity of Sal, but also provided new insights of Sal combined with autophagy inhibitors

as adjuvant chemotherapy strategy for human HCC. However, this study only studied the role of one inhibitor in a single cell line. Therefore, further research is needed to obtain more data to explore their potential molecular mechanisms.

Figure 20 Schematic model revealing the potential pathway related to Sal-induced apoptosis and autophagy. Sal (a active compound extracted from the rhizome of *Rhodiola rosea* L) treatment results in mitochondrial apoptosis of HepG2 cells through PI3K-AKT signaling pathway, which damages morphology, and function. Meanwhile, Sal also regulates PI3K-AKT-mTOR signaling pathway to induce cell autophagy, thus improving cell function. Interesting, autophagy inhibitors (CQ) can not only decrese the Sal-induced autophagic flux, but also promote Sal-induced apoptosis. Sal, salidroside. CQ, chloroquine diphosphate.

Abbreviations

Salidroside =Sal; Hepatocellular carcinoma=HCC; Chloroquine diphosphate=CQ; Cell counting kit-8=CCK-8); Inverted microscope=IM; Transmission electron microscope=TEM; Hematoxylin and eosin =H & E; Oral bioavailability=OB; Drug-like=DL; Protein–protein interaction=PPI; Gene ontology =GO; Kyoto encyclopedia of genes and genomes=KEGG; Rapamycin=Rap; Fetal bovine serum =FBS; Reactive oxygen speciesy=ROS; Annexin V=AV; Propidium iodide=PI; Standard deviation=SD; Biological process=BP; Cellular component=CC; Molecular function=MF; Half maximal inhibitory concentration=IC_{50}; Hydrolyze deoxyribonuclease inhibitor =ICAD.

Declarations

Acknowledgements

Not applicable.

Author contributions

HXS: Funding acquisition, supervision, conception and design. BJ: Conducted the majority of the experiments and wrote the original draft. SQH and XFB: Performed the network pharmacology. LLT, YRW, TY and LFF: acquired the experimental data. WJG, YYL and XF: Carried out the data assays. HXS, TW and HG: Interpreted data and critically revised the manuscript.

Funding

This work was supported by the Program of Technology Plan in Gansu Province (No. 18JR2FA010), the Research Project of Traditional Chinese Medicine in Gansu Province (No. GZKP-2021-21), the Natural Science Foundation of Gansu Province (No. 23JRRA1254, 23JRRA1259), and the Lanzhou Science and Technology Plan Project (No. 2023-4-56, No. 2018-1-122).

Availability of data and materials

The data sets used and/or analysed during the current study are available from the corresponding author upon reasonable request.

Declarations

Ethical approval and consent to participate

All procedures were performed in accordance with the Guidelines for the Care and Use of Laboratory Animals of Gansu University of Chinese Medicine and were approved by the Animal Care and Use Committee of Gansu University of Chinese Medicine.

Consent for publication

All the participants have been explained the process and nature of this study and asked to provide oral informed consent.

Competing interests

The authors declare that they have no competing interests.

Author details

[1]Department of Integrated Chinese and Western Medicine, Gansu University of Traditional Chinese Medicine, Lanzhou, Gansu 730000, China. [2]Department of Basic Medicine, Gansu University of Traditional Chinese Medicine, Lanzhou, Gansu 730000, China. [3]Department of Gynecological Oncology, Gansu Provincial Cancer Hospital, Lanzhou, Gansu 730050, China. [4]Translational Medicine Research Center, Gansu Provincial Academic Institute for Medical Research, Gansu Provincial Cancer Hospital, Lanzhou, Gansu 730050, China.

References

1. Siegel RL, Miller KD, Wagle NS, Jemal A. Cancer statistics, 2023. CA Cancer J Clin. 2023;73:17–48.
2. Ikeda M, Morizane C, Ueno M, Okusaka T, Ishii H, Furuse J. Chemotherapy for hepatocellular carcinoma: current status and future perspectives. Jpn J Clin Oncol. 2018;48:103–14.
3. Kudo M. Targeted and immune therapies for hepatocellular carcinoma: Predictions for 2019 and beyond. World J Gastroenterol. 2019;25:789–807.
4. Shin JW, Chung Y-H. Molecular targeted therapy for hepatocellular carcinoma: current and future. World J Gastroenterol. 2013;19:6144–55.
5. Marin JJG, Briz O, Herraez E, Lozano E, Asensio M, Di Giacomo S, et al. Molecular bases of the poor response of liver cancer to chemotherapy. Clin Res Hepatol Gastroenterol. 2018;42:182–92.
6. Tian Y, Tang GJ, Wang JT, Su S, Song M, Li YL. Chemotherapeutic drugs in the treatment of hepatocellular carcinoma:research advances. J Inter Pharma Res. 2020;47:1088–93.

7. Sun AH, Chen J, Guan H M, Li P. Reversal effect of paeonol on multidrug resistance of liver cancer cell line HepG2/ADM. Shandong Med J. 2016;56:1–4.
8. Kerr JF, Wyllie AH, Currie AR. Apoptosis: a basic biological phenomenon with wide-ranging implications in tissue kinetics. Br J Cancer. 1972;26:239–57.
9. Parzych KR, Klionsky DJ. An overview of autophagy: morphology, mechanism, and regulation. Antioxid Redox Signal. 2014;20:460–73.
10. Wang Y, Liu CY, Wang ZY, Song FM, Meng XL, Yu JH, et al. Pseudolaric acid B induced autophagy through DNA damage response to inhibit apoptosis. Jilin J Chin Med. 2017;37:381–4.
11. Shi Y, Han JJ, Tennakoon JB, Mehta FF, Merchant FA, Burns AR, et al. Androgens promote prostate cancer cell growth through induction of autophagy. Mol Endocrinol. 2013;27:280–95.
12. Yang S, Wang X, Contino G, Liesa M, Sahin E, Ying H, et al. Pancreatic cancers require autophagy for tumor growth. Genes Dev. 2011;25:717–29.
13. Zhang P, Sun Y, Yao YY, Liu J. Effects of resveratrol on female reproductive system malignant tumors. J Dalian Med Univ. 2015;37:403–7.
14. Zhan XJ, Xie DZ, Hu YY, Zhao L, Zhou NJ, Dai G. Experimental study on anti-hepatocellular carcinoma and sensitizing effect of matrine combined with 5-fluorouracil in vitro. Jiangxi J Trad Chin Med. 2016;47:42–5.
15. Mai TT, Moon J, Song Y, Viet PQ, Phuc PV, Lee JM, et al. Ginsenoside F2 induces apoptosis accompanied by protective autophagy in breast cancer stem cells. Cancer Lett. 2012;321:144–53.
16. Zhang Y, Bao J, Wang K, Jia X, Zhang C, Huang B, et al. Pulsatilla saponin D inhibits autophagic flux and synergistically enhances the anticancer activity of chemotherapeutic agents against HeLa cells. Am J Chin Med. 2015;43:1657–70.
17. Tang Q, Bu WH, Wang DD, Xin Y, Xu XW, Sun HC. Advance research on interaction between autophagy and apoptosis and its influence in development of tumors. J Jilin Univ (Med Edi). 2015;41:1303–6.
18. Cheng Y, Yang J-M. Autophagy and apoptosis: rivals or mates? Chin J Cancer. 2013;32:103–5.
19. Pinzi L, Rastelli G. Molecular docking: shifting paradigms in drug discovery. Int J Mol Sci. 2019;20:4331.
20. Häcker G. The morphology of apoptosis. Cell Tissue Res. 2000;301:5–17.
21. Ovadje P, Chatterjee S, Griffin C, Tran C, Hamm C, Pandey S. Selective induction of apoptosis through activation of caspase-8 in human leukemia cells (Jurkat) by dandelion root extract. J Ethnopharmacol. 2011;133:86–91.
22. Ogretmen B. Sphingolipid metabolism in cancer signalling and therapy. Nat Rev Cancer. 2018;18:33–50.
23. Heo J-M, Rutter J. Ubiquitin-dependent mitochondrial protein degradation. Int J Biochem Cell Biol. 2011;43:1422–6.

24. Wu H, Che X, Zheng Q, Wu A, Pan K, Shao A, et al. Caspases: a molecular switch node in the crosstalk between autophagy and apoptosis. Int J Biol Sci. 2014;10:1072–83.
25. Kibble M, Saarinen N, Tang J, Wennerberg K, Mäkelä S, Aittokallio T. Network pharmacology applications to map the unexplored target space and therapeutic potential of natural products. Nat Prod Rep. 2015;32:1249–66.
26. Hopkins AL. Network pharmacology: the next paradigm in drug discovery. Nat Chem Biol. 2008;4:682–90.
27. Zhang H, Zhang S, Hu M, Chen Y, Wang W, Zhang K, et al. An integrative metabolomics and network pharmacology method for exploring the effect and mechanism of Radix Bupleuri and Radix Paeoniae Alba on anti-depression. J Pharm Biomed Anal. 2020;189:113435.
28. Niu B, Xie X, Xiong X, Jiang J. Network pharmacology-based analysis of the anti-hyperglycemic active ingredients of roselle and experimental validation. Comput Biol Med. 2022;141:104636.
29. Wu Y, Liu X, Li G. Integrated bioinformatics and network pharmacology to identify the therapeutic target and molecular mechanisms of Huangqin decoction on ulcerative Colitis. Sci Rep. 2022;12:159.
30. Galluzzi L, Bravo-San Pedro JM, Demaria S, Formenti SC, Kroemer G. Activating autophagy to potentiate immunogenic chemotherapy and radiation therapy. Nat Rev Clin Oncol. 2017;14:247–58.
31. Wang YW, Hou JS. Function of autophagy gene Beclin 1 in tumor and its relationship with oral cancer. Chin J Practical Stoma. 2011;4:374–6.
32. Fu J, Shang H-X, Jia H-T. [Relationship of beclin1 with autophagy and tumor]. Sheng Li Ke Xue Jin Zhan. 2012;43:155–8.
33. Zheng Q, Su H, Ranek MJ, Wang X. Autophagy and p62 in cardiac proteinopathy. Circ Res. 2011;109:296–308.
34. Li XY, Zhao WD, Zhou Y, Tao F, Xu HJ. Expression of autophagy marker protein p62 in cervical squamous cell cancer and its clinical significance. Chin J Clinical Exper Path. 2014;30:38–41.
35. Kabeya Y, Mizushima N, Yamamoto A, Oshitani-Okamoto S, Ohsumi Y, Yoshimori T. LC3, GABARAP and GATE16 localize to autophagosomal membrane depending on form-II formation. J Cell Sci. 2004;117:2805–12.
36. Zhao Y, Li R, Xia W, Neuzil J, Lu Y, Zhang H, et al. Bid integrates intrinsic and extrinsic signaling in apoptosis induced by alpha-tocopheryl succinate in human gastric carcinoma cells. Cancer Lett. 2010;288:42–9.
37. Estaquier J, Vallette F, Vayssiere J-L, Mignotte B. The mitochondrial pathways of apoptosis. Adv Exp Med Biol. 2012;942:157–83.
38. Labat-Moleur F, Chabre O, Guillermet C, Chaffanjon P, Blumet-Rondeu F, Bauchet A, et al. Graves-Basedow disease goiter: a model of Bax-Bcl2 regulated apoptosis. Thyroid. 1999;9:483–92.
39. Fan T-J, Han L-H, Cong R-S, Liang J. Caspase family proteases and apoptosis. Acta Biochim Biophys Sin (Shanghai). 2005;37:719–27.

40. Van Opdenbosch N, Lamkanfi M. Caspases in Cell Death, Inflammation, and Disease. Immunity. 2019;50:1352–64.
41. Rubinstein AD, Kimchi A. Life in the balance - a mechanistic view of the crosstalk between autophagy and apoptosis. J Cell Sci. 2012;125:5259–68.
42. Noorolyai S, Shajari N, Baghbani E, Sadreddini S, Baradaran B. The relation between PI3K/AKT signalling pathway and cancer. Gene. 2019;698:120–8.
43. Xu C, Sun G, Yuan G, Wang R, Sun X. Effects of platycodin D on proliferation, apoptosis and PI3K/Akt signal pathway of human glioma U251 cells. Molecules. 2014;19:21411–23.
44. Chen LY, Liu Y. Quercitrin promotes apoptosis of gastric cancer cell line SGC7901 by inhibiting PI3K/AKT signaling pathway. Chin J Pathophysiol. 2018;34:1976–80.
45. Fu WW, Ou YYR, Huang CY, Huang JW, Lu S, Huang DH, et al. Research progress in the treatment of cardiovascular diseases based on mTOR regulating autophagy. J Hainan Med Univ. 2021;27:635–40.
46. Kim K-Y, Park K-I, Kim S-H, Yu S-N, Park S-G, Kim YW, et al. Inhibition of autophagy promotes salinomycin-induced apoptosis via reactive oxygen species-mediated PI3K/AKT/mTOR and ERK/p38 MAPK-dependent signaling in human prostate cancer cells. Int J Mol Sci. 2017;18:1088.
47. Rong L, Li Z, Leng X, Li H, Ma Y, Chen Y, et al. Salidroside induces apoptosis and protective autophagy in human gastric cancer AGS cells through the PI3K/Akt/mTOR pathway. Biomed Pharmacother. 2020;122:109726.

Tables

Table 1 Active ingredients and ADME parameters of *Rhodiola rosea* L.

MOL ID	Name of ingredients	Formula	OB%	DL
MOL000244	Borneol	$C_{10}H_{18}O$	81.8	0.05
MOL004479	O-cresol	C_7H_8O	62.45	0.02
MOL004358	Linalool	$C_{10}H_{18}O$	58.18	0.02
MOL000098	Quercetin	$C_{15}H_{10}O_7$	46.43	0.28
MOL000771	p-coumaric acid	$C_9H_8O_3$	43.29	0.04
MOL000422	Kaempferol	$C_{15}H_{10}O_6$	41.88	0.24
MOL001442	Phytol	$C_{20}H_{40}O$	33.82	0.13
MOL000513	Gallic acid	$C_7H_6O_5$	31.69	0.04
MOL002083	Tricin	$C_{17}H_{14}O_7$	27.86	0.34
MOL002558	Umbelliferone	$C_9H_6O_3$	27.37	0.05
MOL001907	Ethyl gallate	$C_9H_{10}O_5$	25.61	0.06
MOL000197	Myrcene	$C_{10}H_{16}$	24.96	0.02
MOL000123	Geraniol	$C_{10}H_{18}O$	23.93	0.02
MOL000124	Citral	$C_{10}H_{16}O$	22.52	0.02
MOL001285	N-octanol	$C_8H_{18}O$	21.06	0.01
MOL003508	1-decanol	$C_{10}H_{22}O$	16.85	0.02
MOL002929	Salidroside	$C_{14}H_{20}O_7$	15.96	0.2
MOL003426	Salipurposide	$C_{21}H_{22}O_{10}$	15.6	0.75
MOL000865	N-cetane	$C_{16}H_{34}$	15.6	0.06
Not detected	Kaempferol-10-rhamnoside	—	—	—
Not detected	Kaempferol-8-rhamnoside	—	—	—
Not detected	Lemongrass acid	—	—	—

Table 2 Topological analysis of *Rhodiola rosea* L-active ingredients-potential targets network.

Name of ingredients	Degree	Betweenness centrality	Closeness centrality
Quercetin	61	7110.92298	77.16667
Salidroside	16	602.41283	46.5
Geraniol	12	1373.12011	44.5
Lemongrass acid	10	701.05428	43.16667
Tricin	7	96.56614	41.16667
Kaempferol	7	613.76427	41.16667
Phytol	5	62.0037	39.83333
N-cetane	4	228.1157	39.16667
p-coumaric acid	3	15.36136	38.5
Salipurposide	3	11.0238	38.5
O-cresol	2	3.82122	37.83333
N-octanol	2	97	37.83333
Myrcene	2	4.73997	37.83333
Linalool	2	3.82122	37.83333
Citral	2	12.06178	37.83333
Borneol	2	9.04275	37.83333
Umbelliferone	2	196	37.83333
Kaempferol-8-rhamnoside	2	3.82122	37.83333
Kaempferol-10-rhamnoside	2	4.73997	37.83333
Gallic acid	2	3.82122	37.83333
Ethyl gallate	2	3.78545	37.83333
1-decanol	2	97	37.83333

Figures

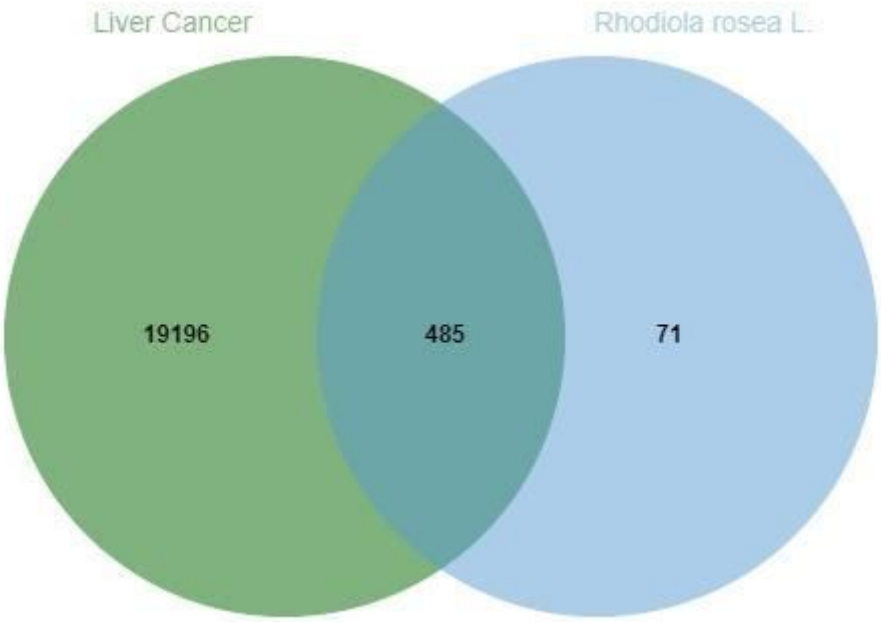

Figure 1

Venn diagram of overlapping targets between drug and disease.

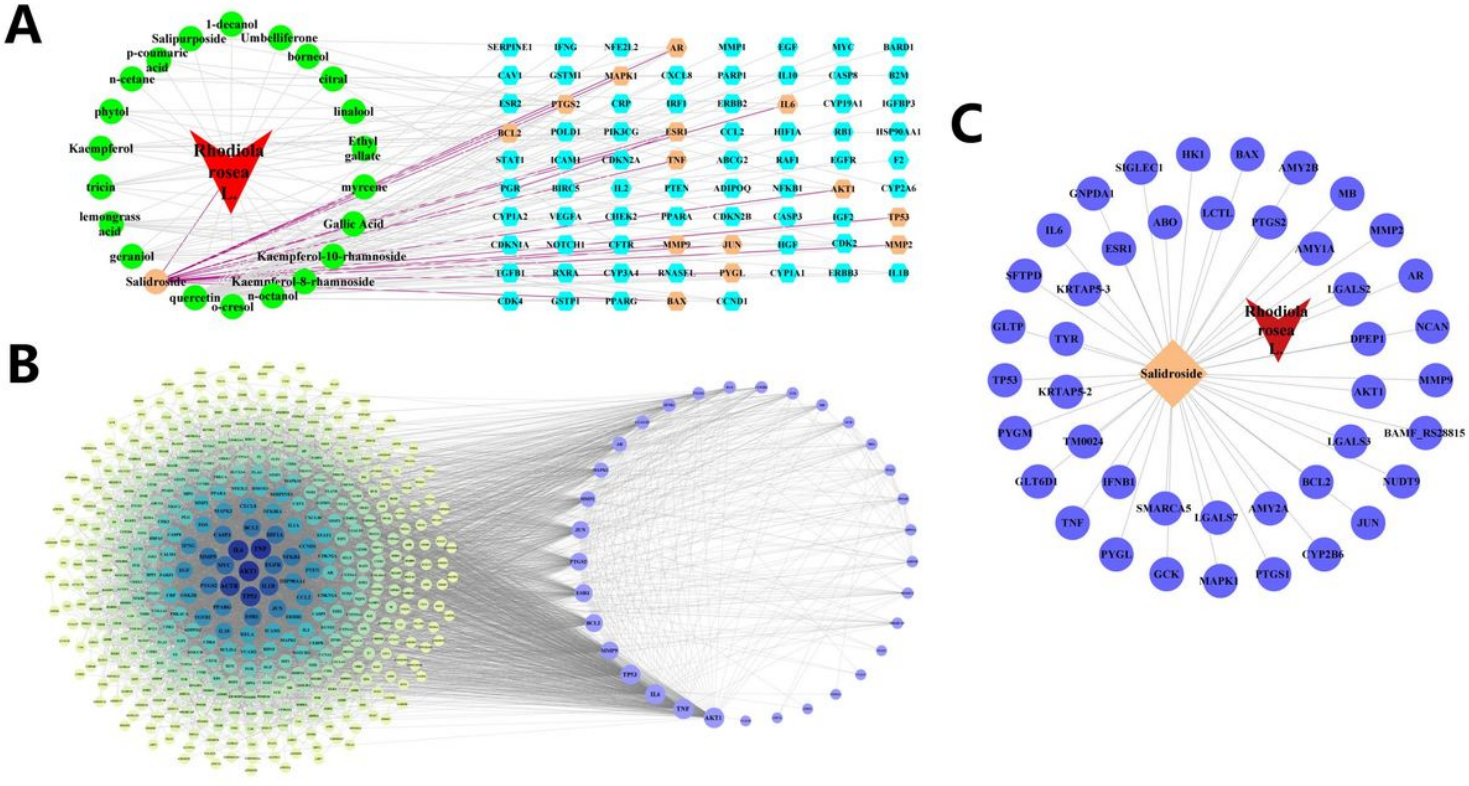

Figure 2

Construction of a “traditional Chinese medicine-active ingredients-diseases-potential targets” network. (A and B) Construction of a “*Rhodiola rosea* L-active ingredients-liver cancer-potential targets” network. (C)

Construction of a "*Rhodiola rosea* L-Sal-liver cancer-potential targets" network. Sal, salidroside.

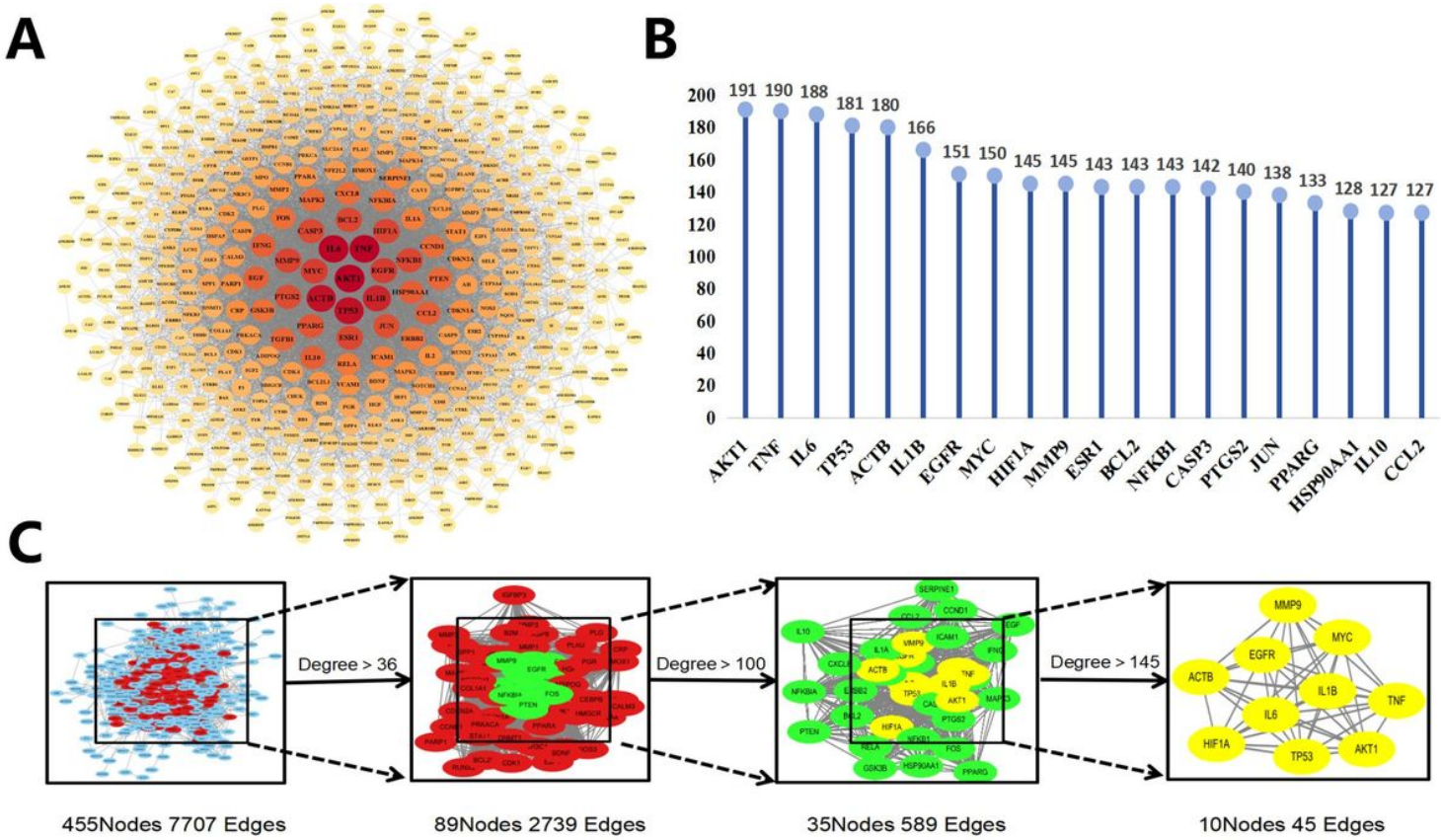

Figure 3

Network topological analysis between "protein-protein". (A) PPI network of potential targets (the size and color depth of nodes are proportional to the degree value). (B) Point bar graph of degree-value points for 20 key targets. (C) Key targets screening process. Among the selected key targets, the top 10 targets with the degree value are represented by yellow. The thickness and color depth of the edge are directly proportional to the correlation between the targets. PPI, protein-protein interaction.

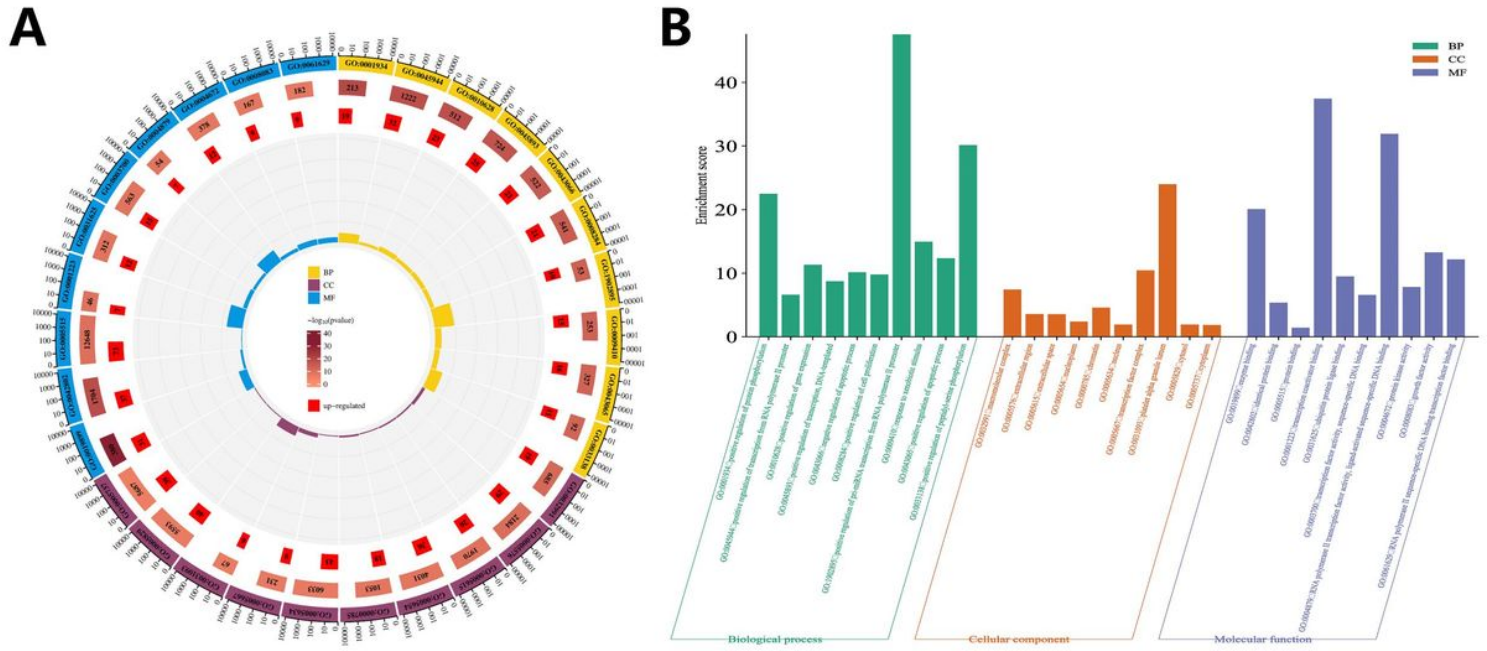

Figure 4

Enrichment analysis of the GO organisms. (A) Concentric circle plot of GO biological enrichment analysis. (B) Histogram of the GO biological enrichment analysis. GO, gene ontology.

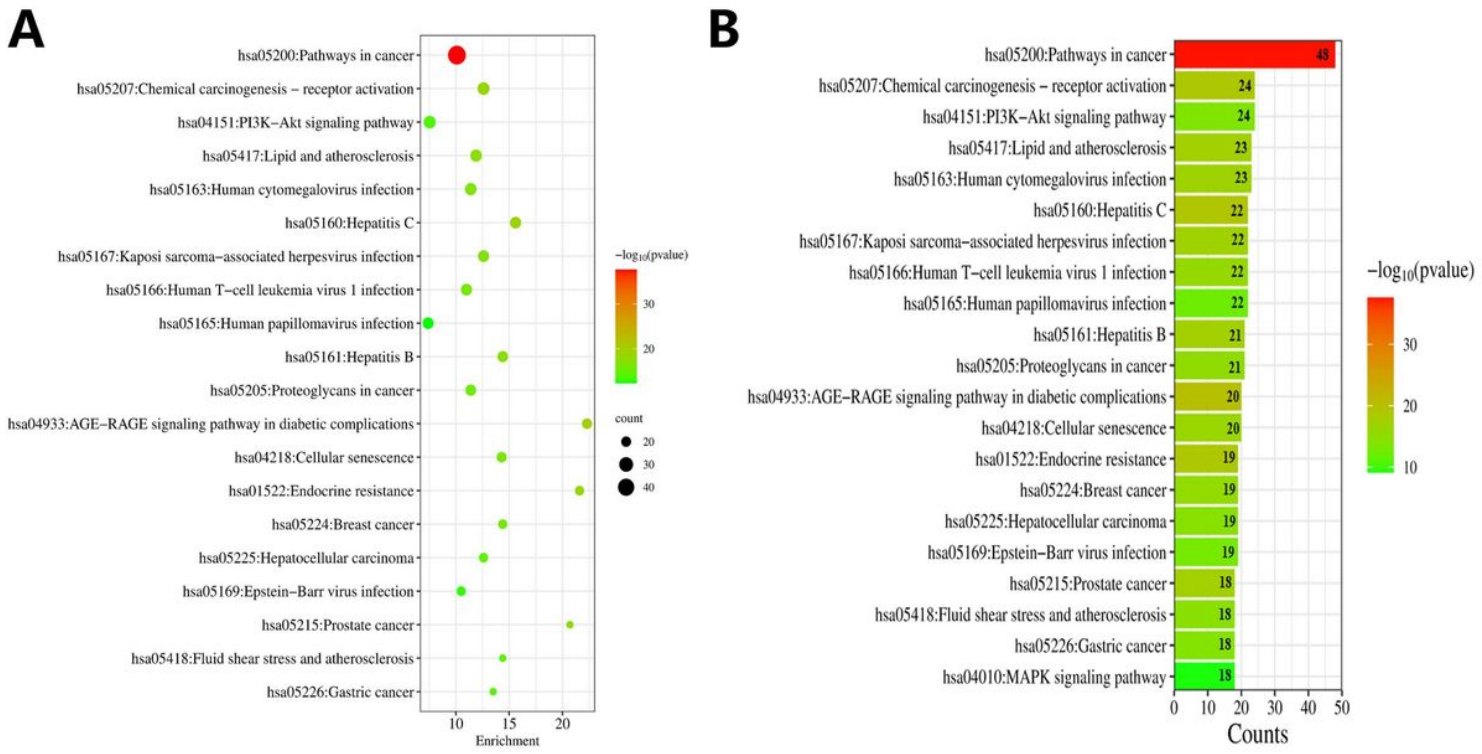

Figure 5

Enrichment analysis of the KEGG pathways. (A) Bubble diagram of KEGG pathway enrichment analysis. (B) KEGG pathway classification diagram. KEGG, kyoto encyclopedia of genes and genomes.

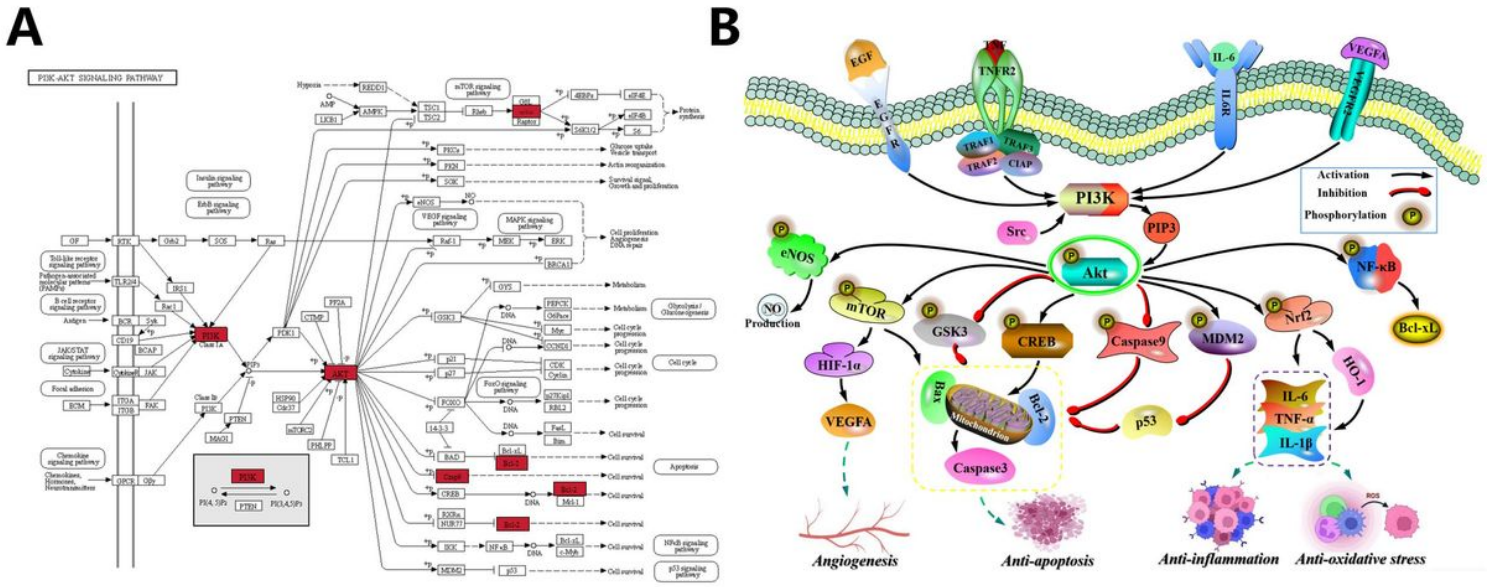

Figure 6

Molecular mechanism diagram of predicting drug therapy for disease. (A and B) Predicted mechanism of potential targets of Sal for HCC treatment via the PI3K/AKT signaling pathway. Sal, salidroside; HCC, hepatocellular carcinoma.

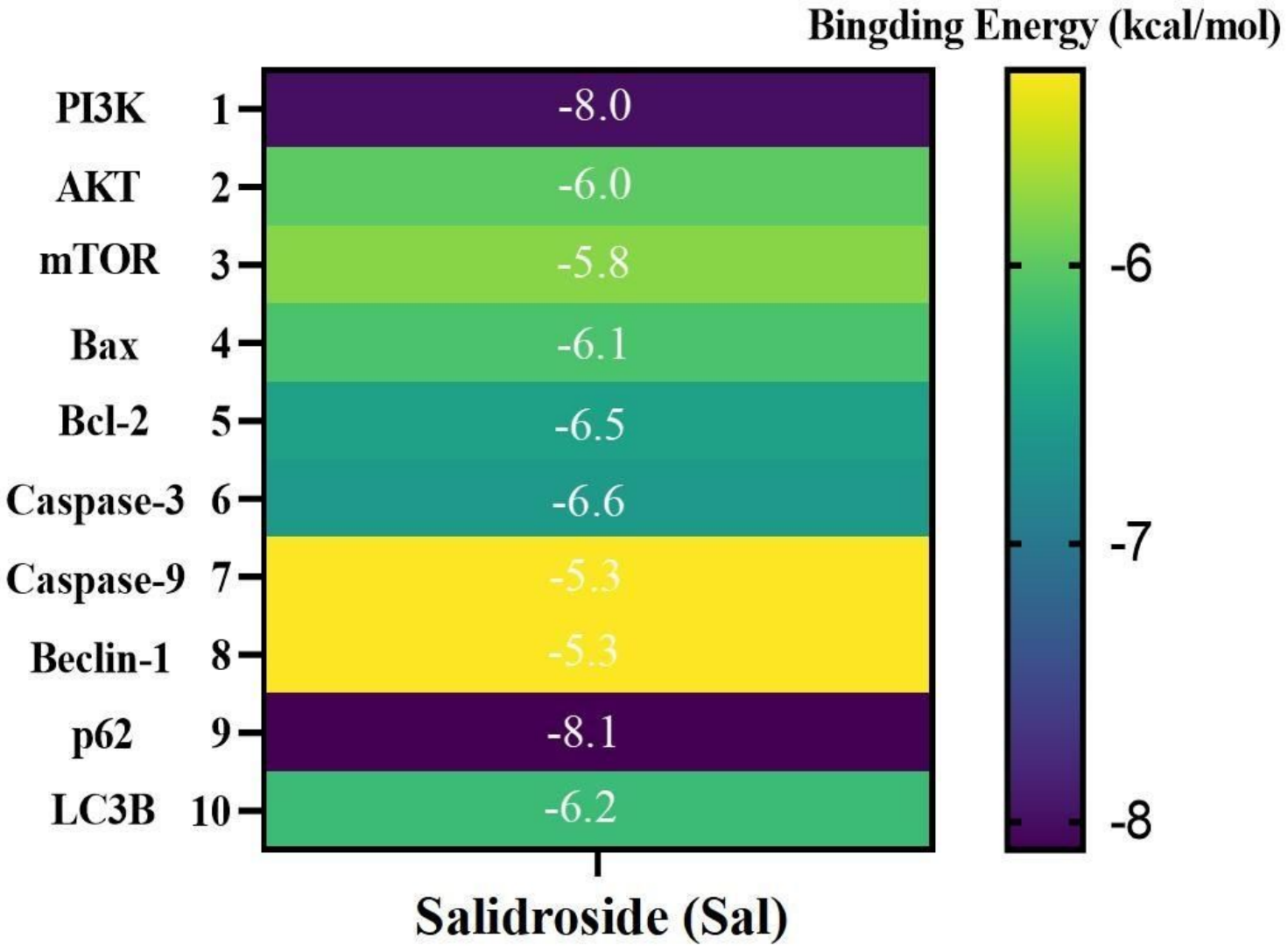

Figure 7

Molecular docking binding energy heatmap (the color shade is inversely proportional to the magnitude of the binding energy).

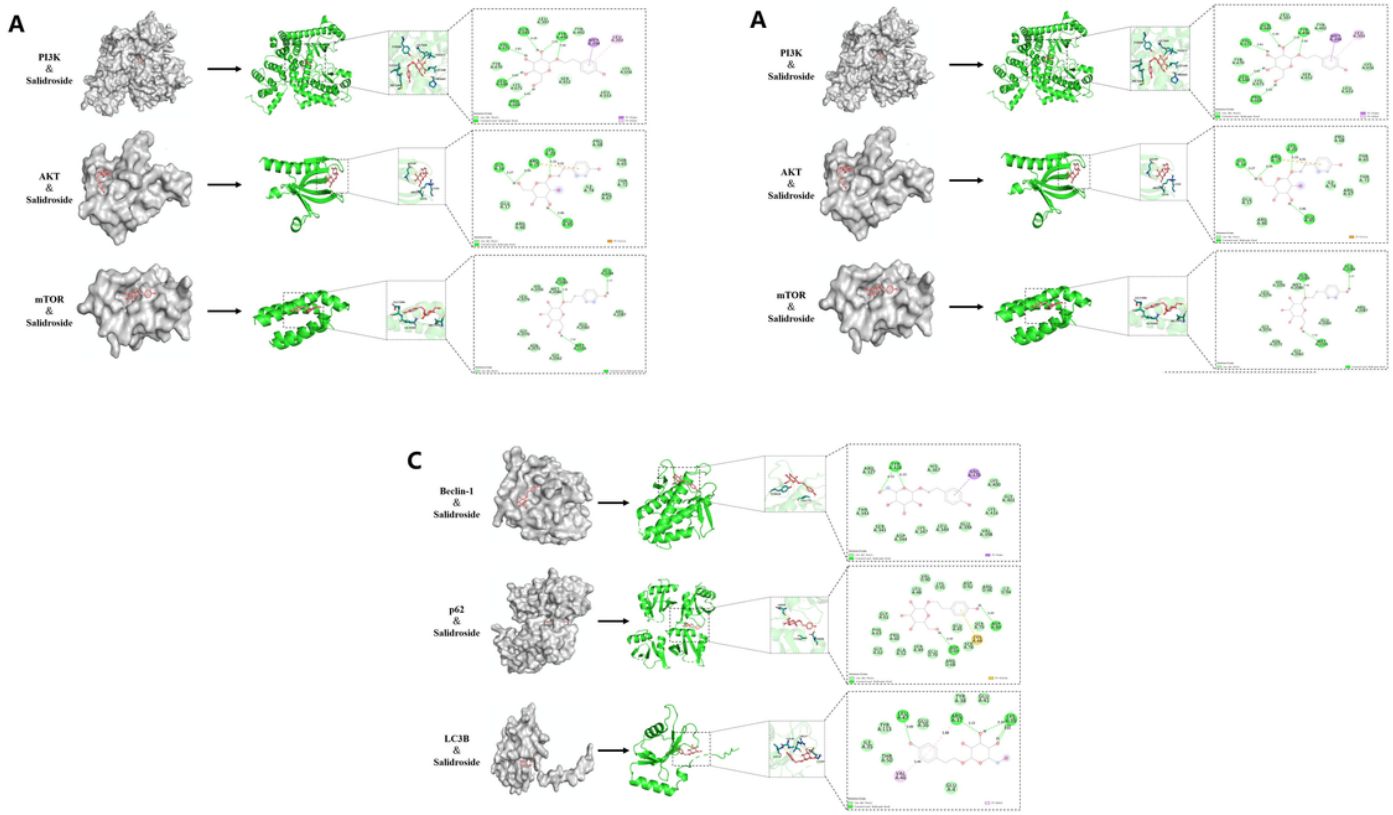

Figure 8

Molecular docking analysis of Sal to key targets. (A) Signaling pathway-related targets (including PI3K, AKT and mTOR)–Sal interaction surface and 2D and 3D images of the molecular docking results. (B) Mitochondrial apoptosis-related targets (including Bax, Bcl-2, Caspase-3 and Caspase-9)–Sal interaction surface and 2D and 3D images of the molecular docking results. (C) Autophagy-related targets (including Beclin-1, p62 and LC3B)–Sal interaction surface and 2D and 3D images of the molecular docking results. Sal, salidroside.

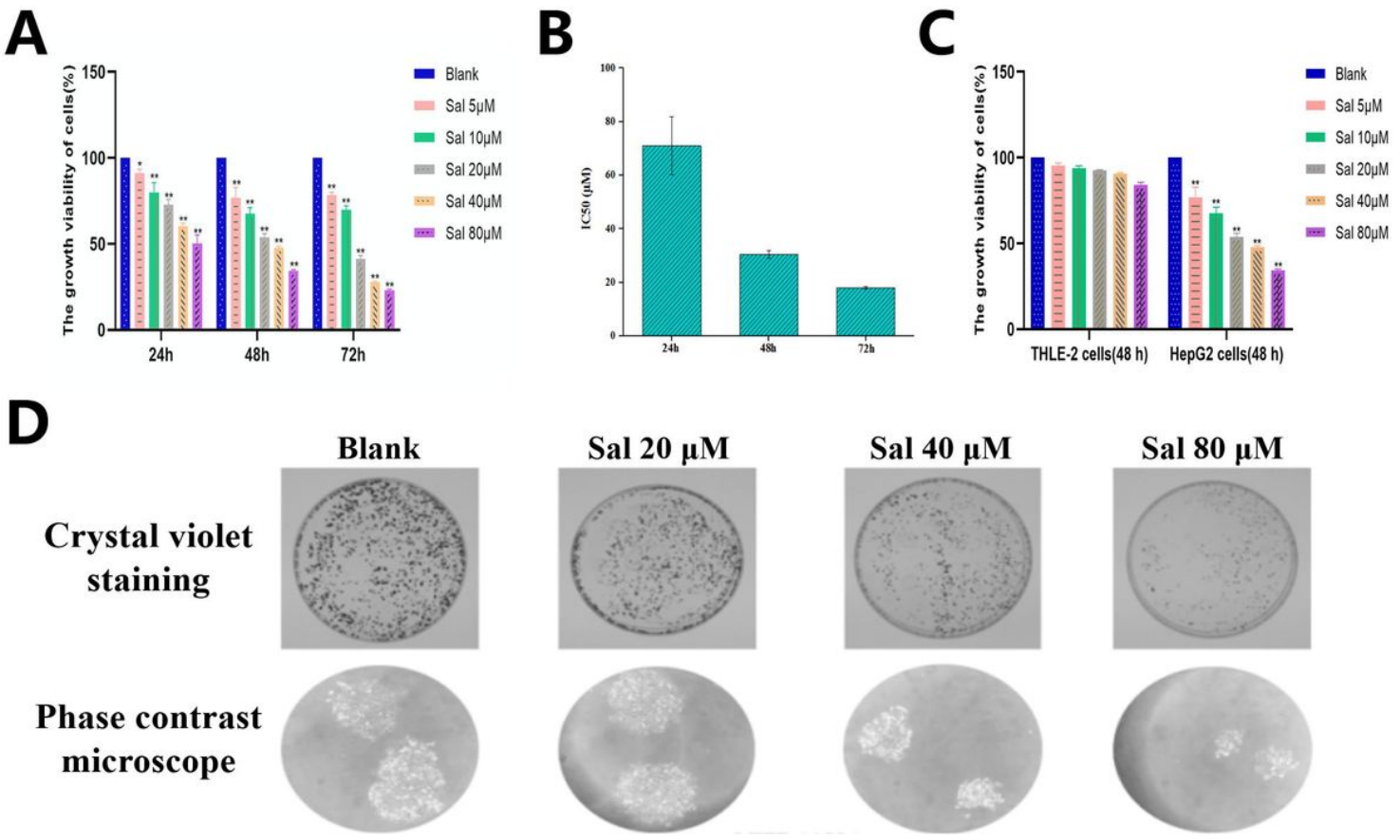

Figure 9

Sal-suppressed viability and proliferation in HepG2 cells. (A) The effects of Sal at various concentrations on the proliferation in HepG2 cells by CCK-8 method. $^{*}P<0.05$, $^{**}P<0.01$ vs. blank. (B) The results of IC_{50} in Sal-treated HepG2 cells by CCK-8 method. (C) The toxicological effects of Sal on human liver normal cells THLE-2 by CCK-8 method. $^{**}P<0.01$ vs. blank. (D) The effects of Sal on the proliferative ability in HepG2 cells were observed by the plate colony formation experiment. Magnification, x40, x200. Sal, salidroside; IC_{50}, half maximal inhibitory concentration.

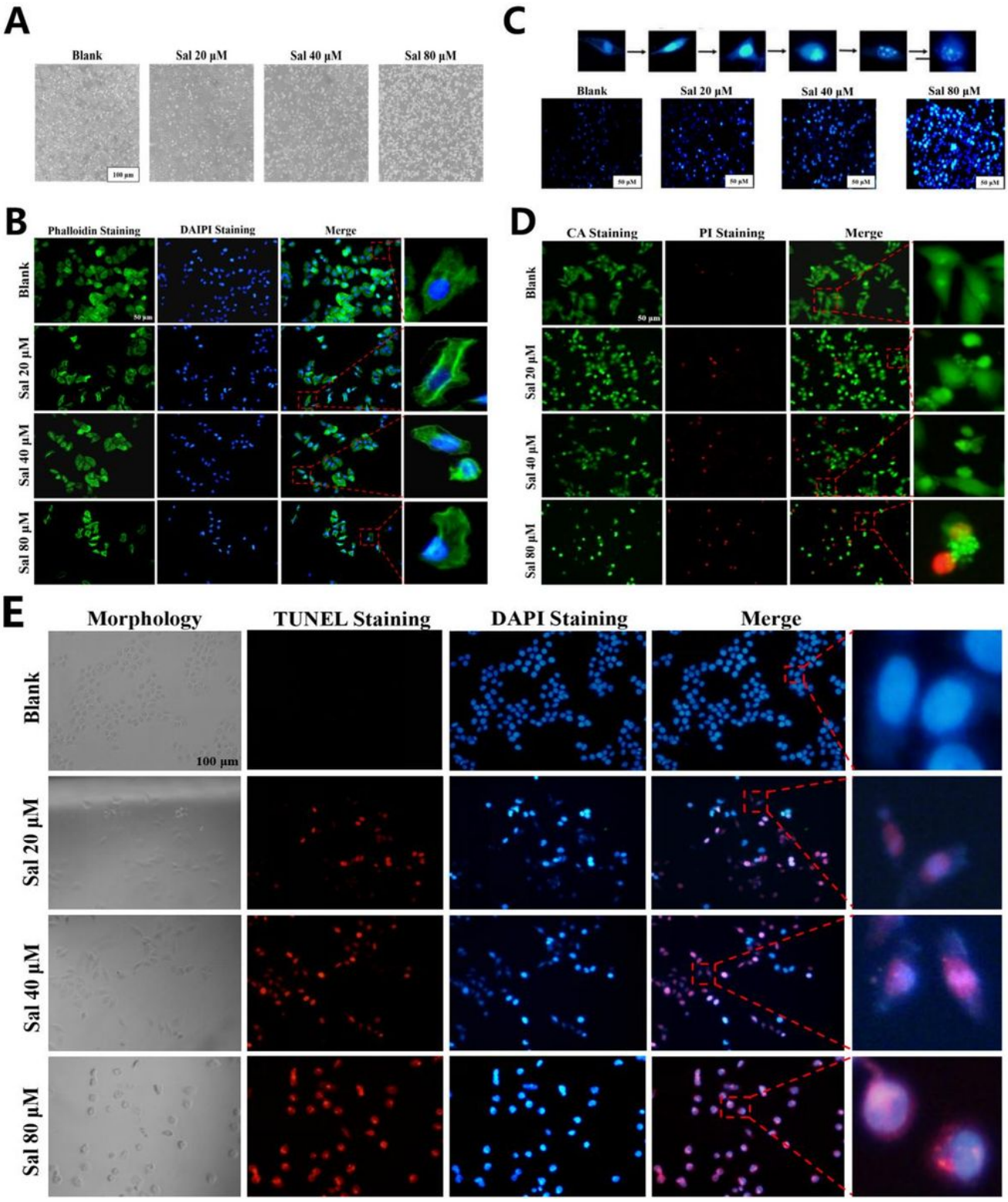

Figure 10

Sal-induced apoptosis in HepG2 cells. (A and B) The cellular morphology after Sal treated was observed by using IM and phalloidin staining. Magnification, ×100. (C, D and E) The phenomenon of apoptosis after Sal treated was observed by using Hoechst33342 staining, Calcein/PI staining and TUNEL staining. Magnification, ×100. Sal, salidroside; IM, inverted microscope.

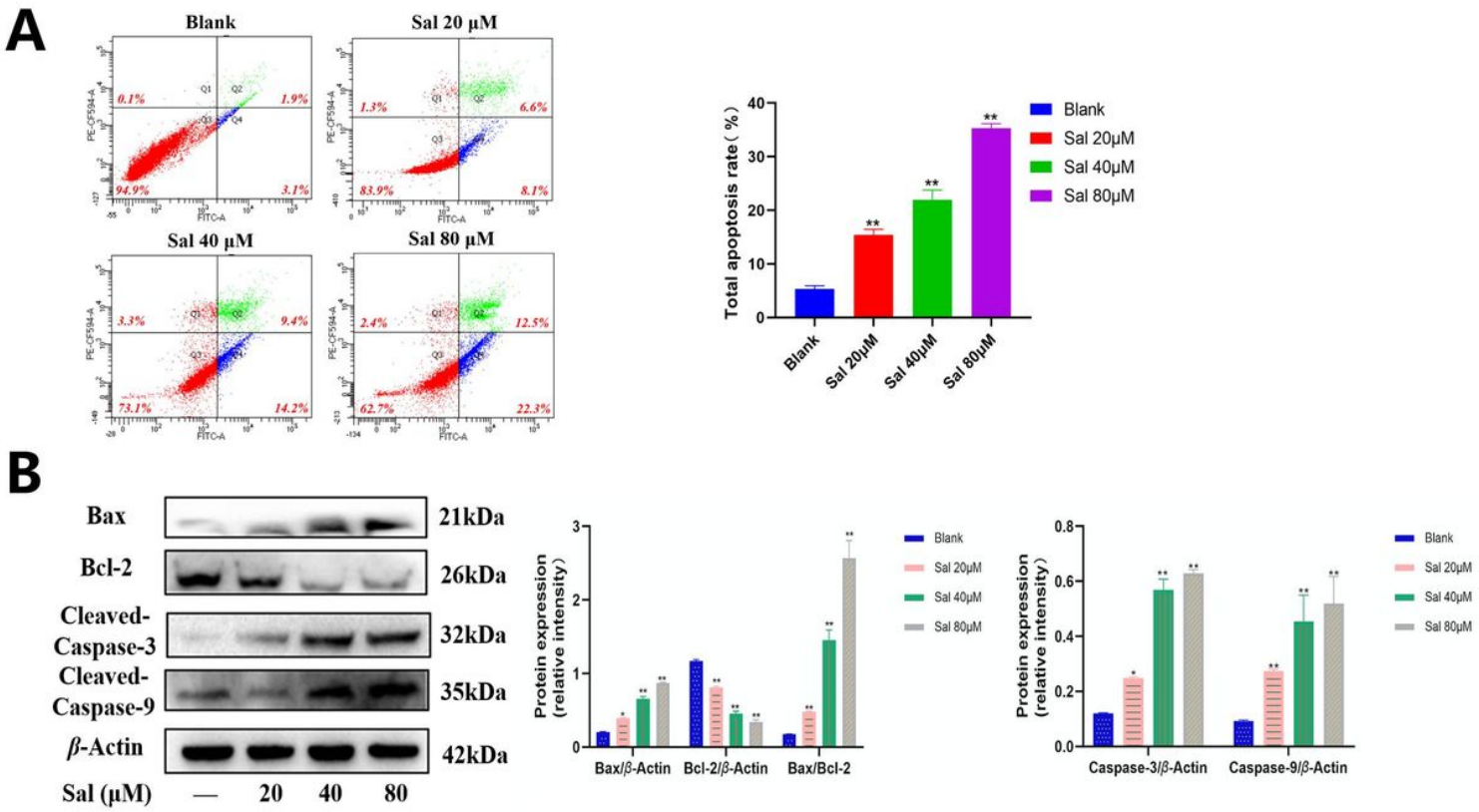

Figure 11

Sal-induced mitochondrial apoptosis in HepG2 cells. (A) The total apoptotic rate after Sal treated was detected by using the flow cytometry. *$^{*}P<0.05$*, *$^{**}P<0.01$* vs. blank. (B) The expression levels of Bax, Bcl-2, cleaved-Caspase-3 and cleaved-Caspase-9 proteins were analyzed by western blotting in HepG2 cells of each group. *$^{*}P<0.05$*, *$^{**}P<0.01$* vs. blank. Sal, salidroside.

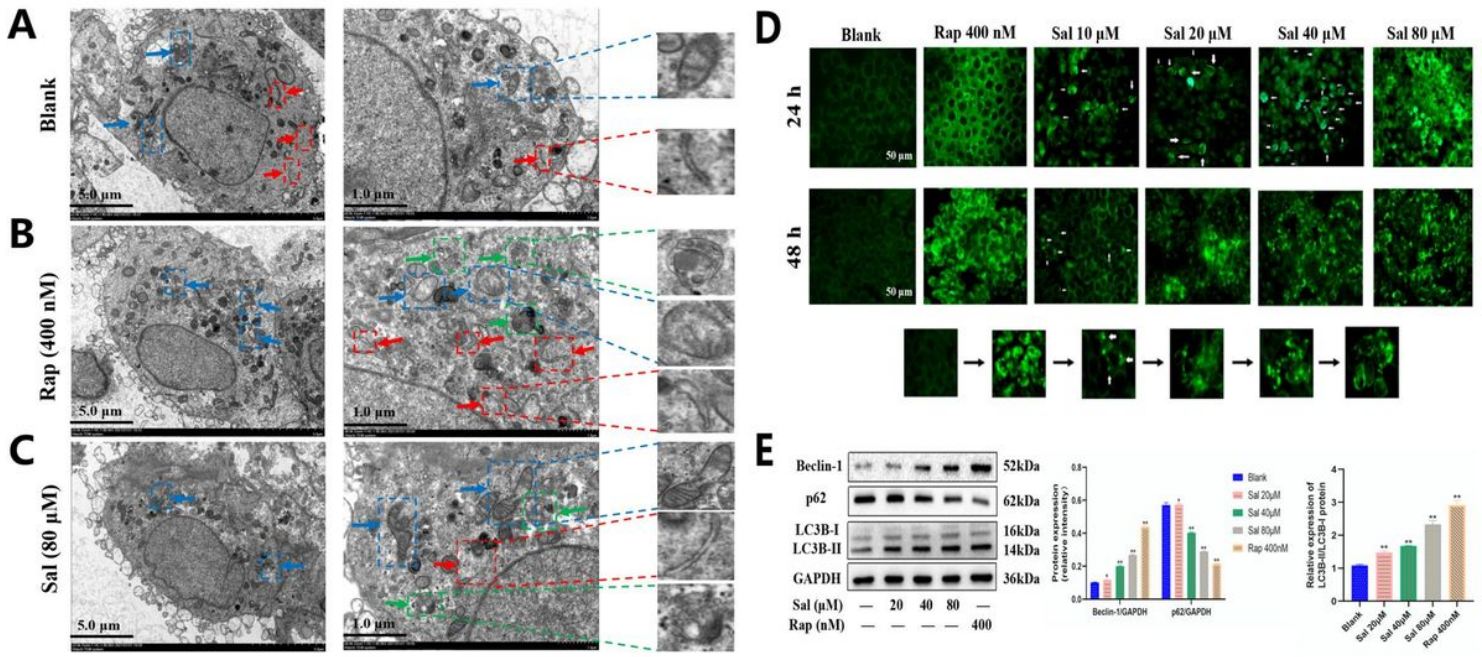

Figure 12

Sal-induced autophagy in HepG2 cells. (A) Untreated HepG2 cells were obtained by TEM. The structures of endoplasmic reticulum and mitochondria were normal in blank group. (B and C) Swollen endoplasmic reticulum and mitochondria were appeared in Rap or Sal treatment group. In addition, autophagosomes in the cytoplasm were also appeared in Rap or Sal treatment group. Red, blue and green arrowheads respectively indicate the endoplasmic reticulum, mitochondria and autophagosomes. Magnification, ×3,000, ×8,000. (D) The green fluorescence related to autophagosomes was increased with a dose-dependent manner in Sal or Rap treatment group by using MDC staining, compared with those in blank group. Magnification, ×200. (E) The expression levels of Beclin-1, p62, LC3B-I and LC3B-II proteins were analyzed by western blotting in HepG2 cells of each group. $^{*}P<0.05$, $^{**}P<0.01$ vs. blank. TEM, transmission electron microscope; Sal, salidroside; Rap, rapamycin.

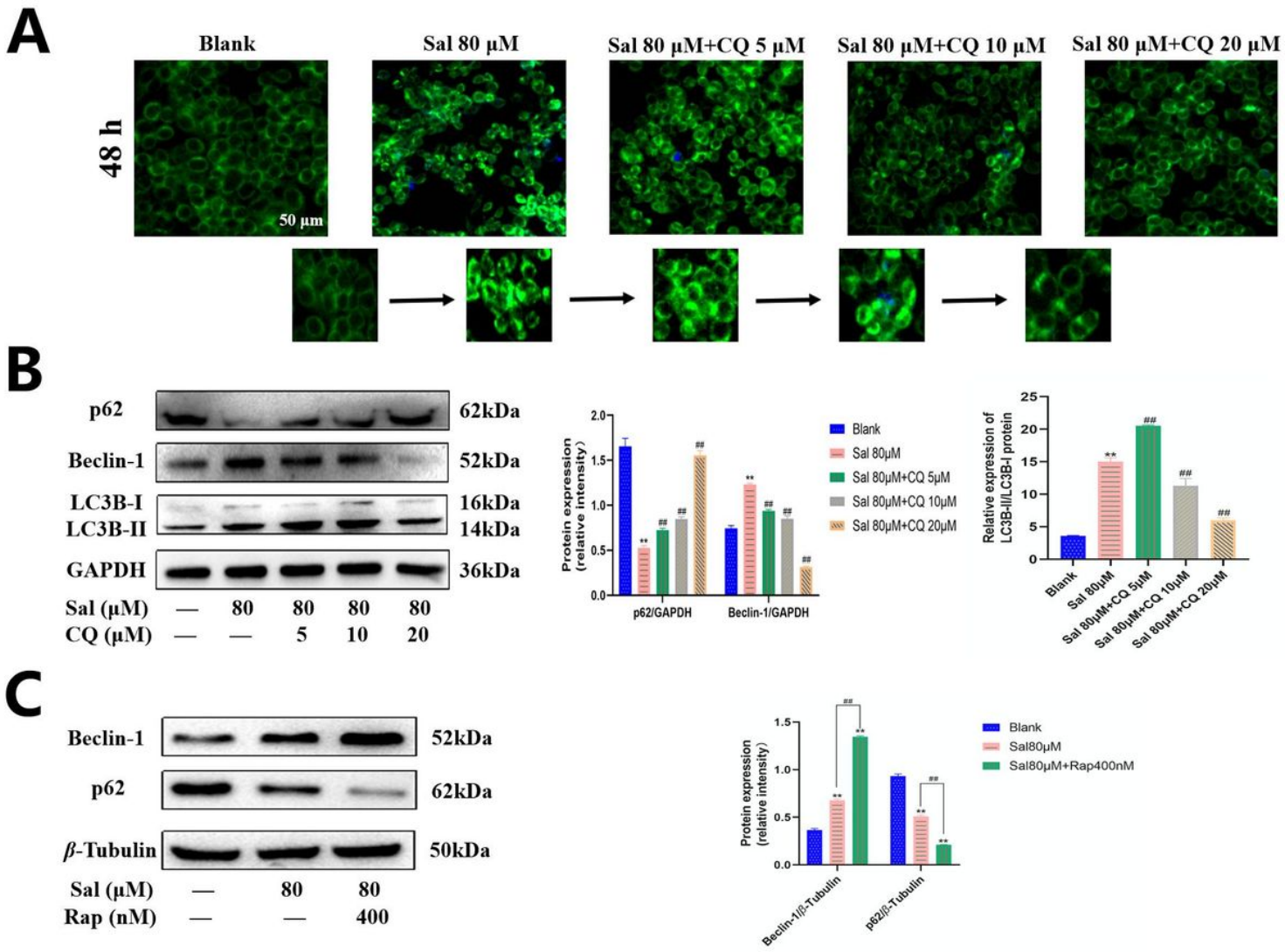

Figure 13

CQ inhibited the Sal-induced autophagy in HePG2 cells. (A) The green fluorescence related to autophagosomes was decreased with a dose-dependent manner in the Sal + CQ group by using MDC staining, compared with the blank and Sal groups. Magnification, ×200. (B and C) The expressions of

Beclin-1, p62, LC3B-I and LC3B-II proteins were analyzed by western blotting in HepG2 cells of each group. $^{**}P<0.01$ vs. blank. $^{\#\#}P<0.01$ vs. Sal group. Sal, salidroside; CQ, chloroquine diphosphate; Rap, rapamycin.

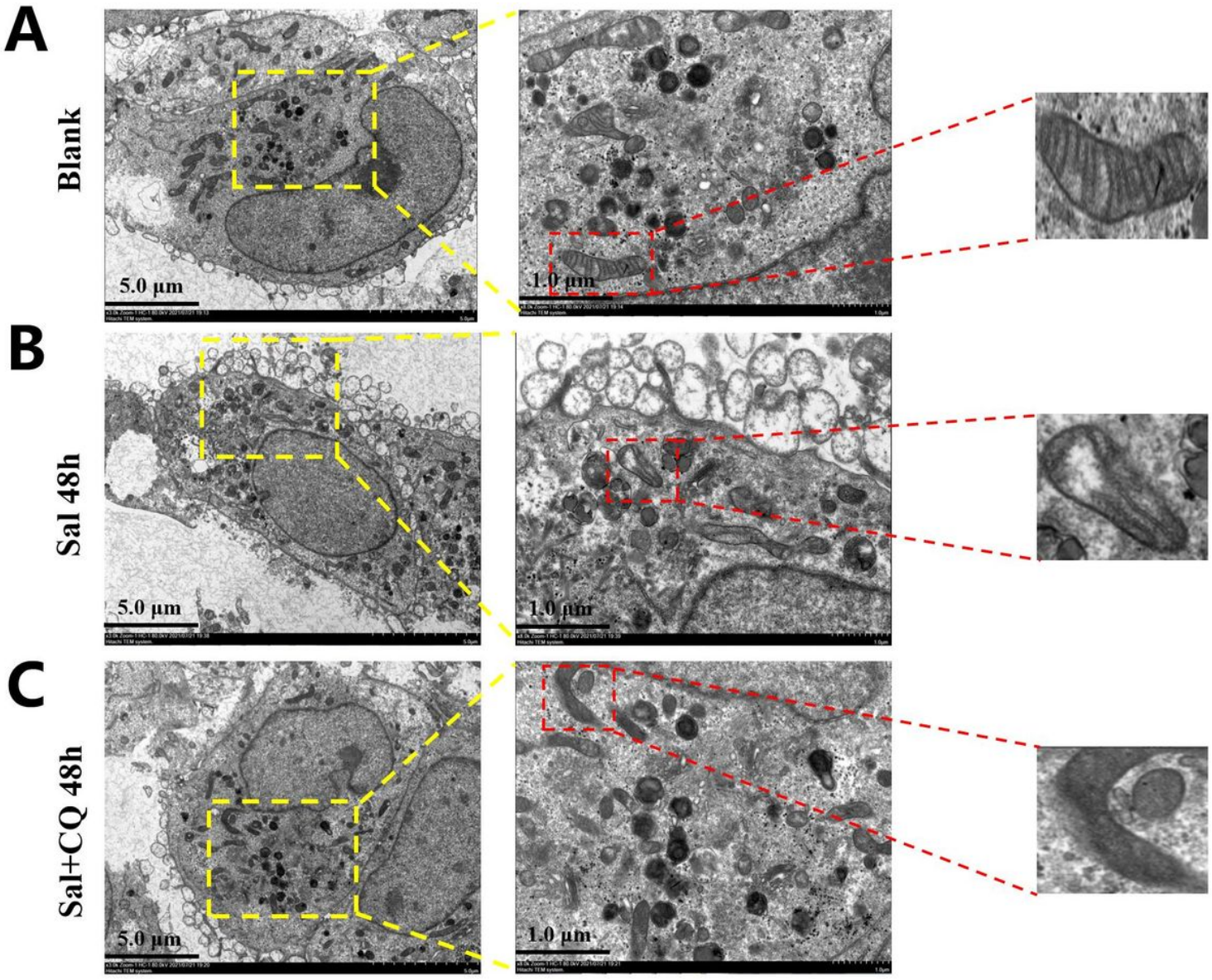

Figure 14

Inhibiting autophagy increased mitochondrial damage in HepG2 cells. The micro-structure of mitochondria in each group were observed by TEM: (A) The morphology of mitochondria was normal in blank group. (B) The mitochondrial swellings were observed following Sal treatment for 48 h in HepG2 cells. (C) After cells were treated with Sal and CQ for 48 h, increased damage to mitochondrial morphology was observed compared with those in blank and Sal groups. Magnification, ×3,000, ×8,000. TEM, transmission electron microscope; Sal, salidroside; CQ, chloroquine diphosphate.

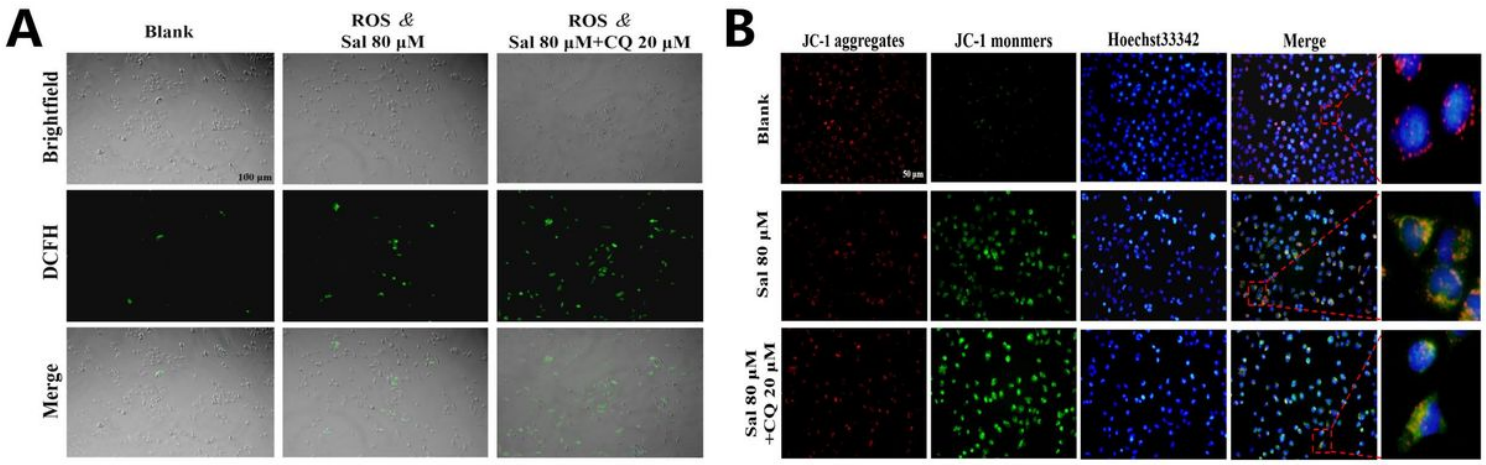

Figure 15

Inhibition of autophagy promoted the degree of mitochondrial dysfunction in HepG2 cells. (A) The content of ROS after Sal and/or CQ treated was observed by using ROSstaining. Magnification, ×100. (B) The changes in mitochondrial membrane potential after Sal and/or CQ treated were observed by using JC-1 staining. Magnification, ×200.

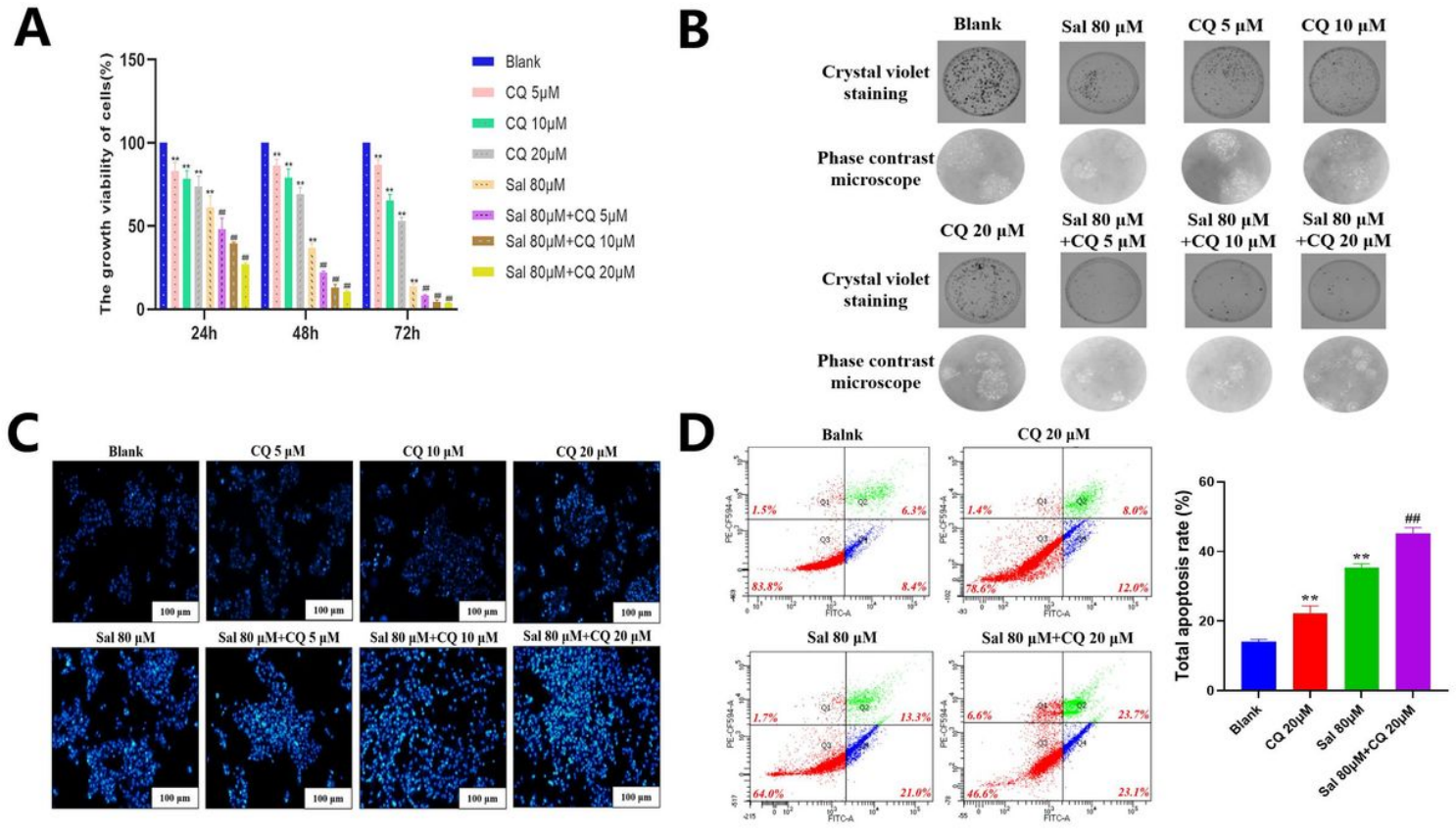

Figure 16

Inhibiting autophagy could improve Sal-induced apoptosis in HepG2 cells. (A) The effects of Sal combined with CQ on the growth viability in HepG2 cells were detected by CCK-8 method. $^{**}P<0.01$ vs.

blank. ##*P<0.01* vs. Sal group. (B) The effects of Sal combined with CQ on the proliferative capacity in HepG2 cells were observed by the plate colony formation experiment. Magnification, ×40, ×200. (C) Apoptosis was measured by Hoechst33342 staining in HepG2 cells. Compared with the blank and Sal groups, the number of apoptotic cells were obviously increased with a dose-dependent manner in the Sal+CQ group. Magnification, ×100. (D) The total apoptotic rate after Sal combined with CQ was detected by using the flow cytometry. ******P<0.01* vs. blank. ##*P<0.01* vs. Sal group. Sal, salidroside; CQ, chloroquine diphosphate.

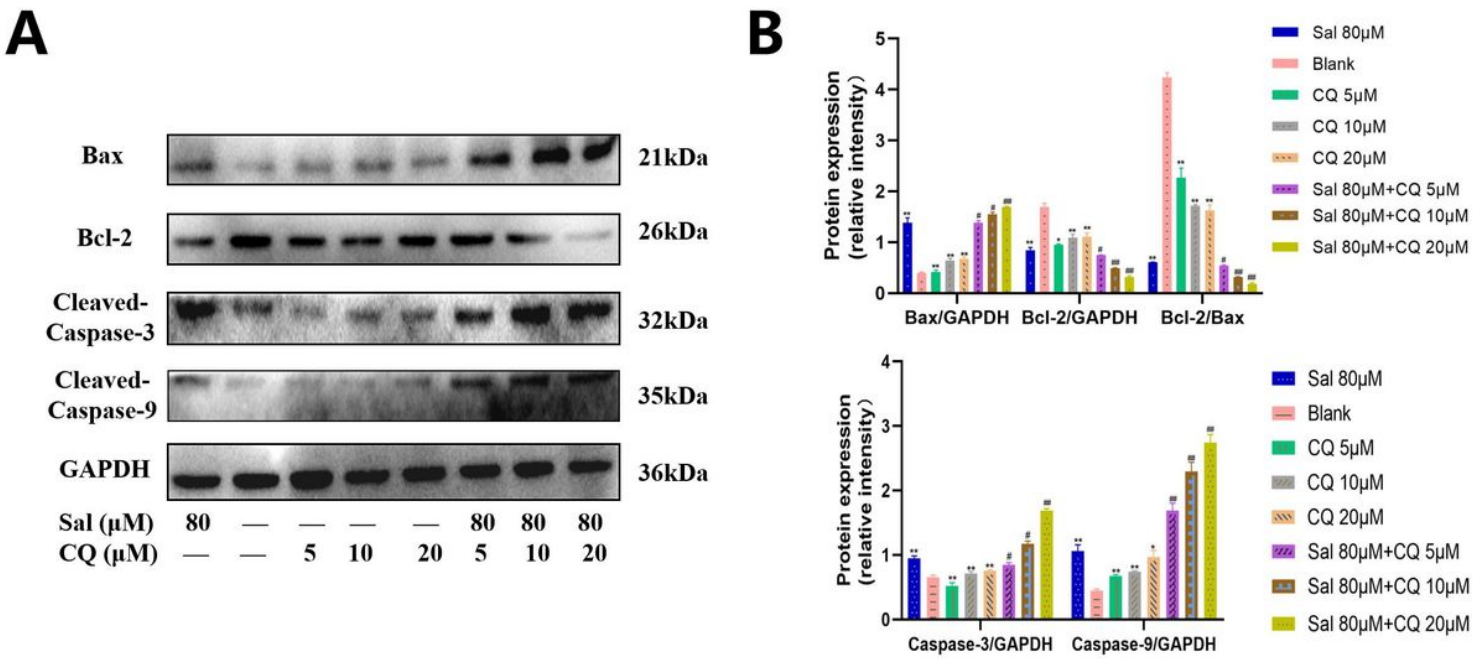

Figure 17

Inhibiting autophagy regulated the expression levels of proteins related to apoptosis in HepG2 cells. (A) The expression levels of Bax, Bcl-2, cleaved-Caspase-3 and cleaved-Caspase-9 proteins were analyzed by western blotting in HepG2 cells of each group. (B) Quantification of Bax, Bcl-2, cleaved-Caspase-3 and cleaved-Caspase-9 proteins by the densitometry. ******P<0.01* vs. blank. #*P<0.05*, ##*P<0.01* vs. Sal group. Sal, salidroside; CQ, chloroquine diphosphate.

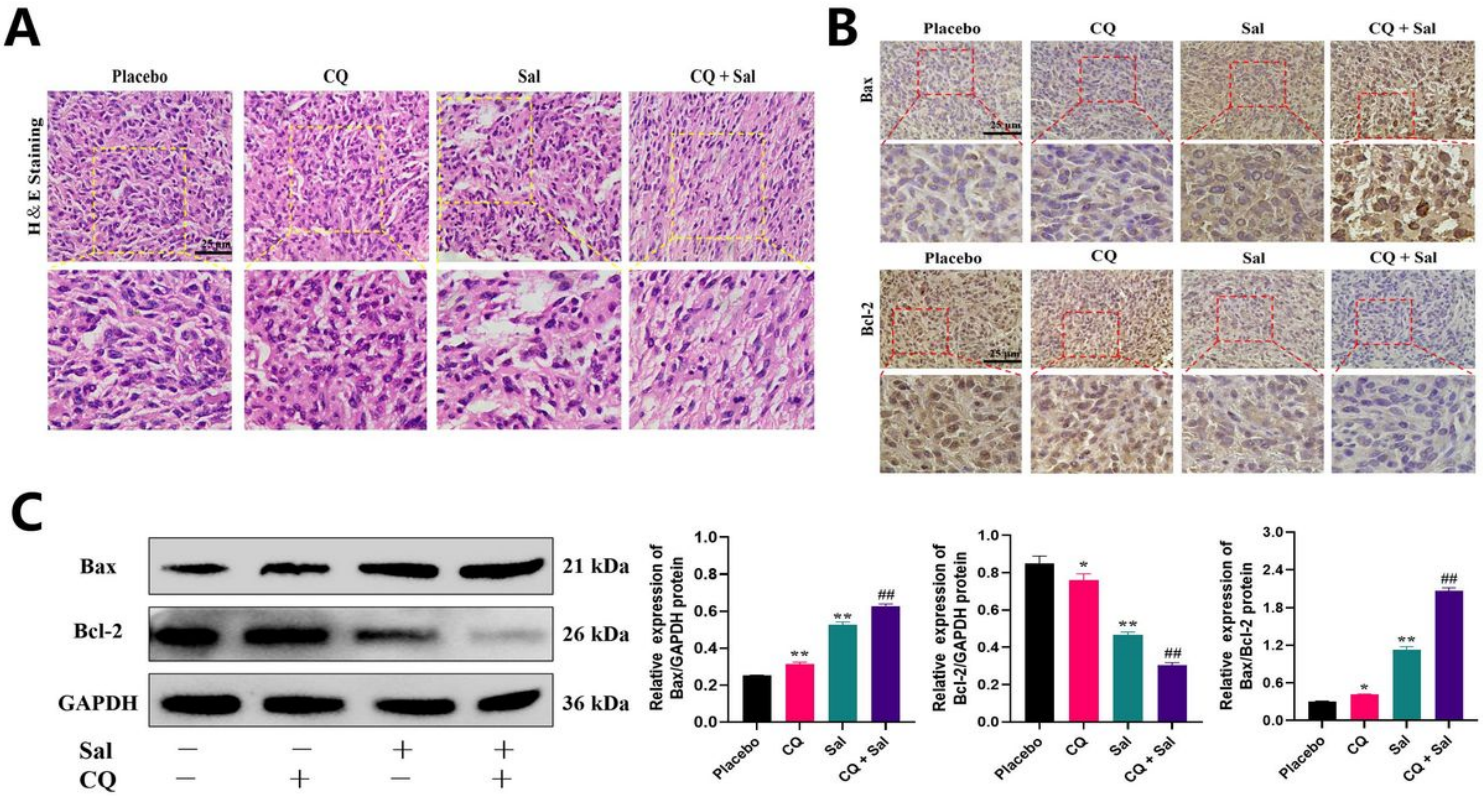

Figure 18

Sal combined with CQ could effectively inhibited tumor formation in mice. (A) The pathological changes of tumor tissues were observed by using H E staining. Magnification, ×400. (B) The expression change of Bax and Bcl-2 proteins were observed by using immunohistochemistry. Magnification, ×400. (C) The expression levels of Bax and Bcl-2 proteins were analyzed by western blotting in tumor tissues of each group. $^{*}P<0.05$, $^{**}P<0.01$ vs. Placebo group. $^{\#\#}P<0.01$ vs. Sal group. Sal, salidroside; CQ, chloroquine diphosphate; H E, hematoxylin and eosin.

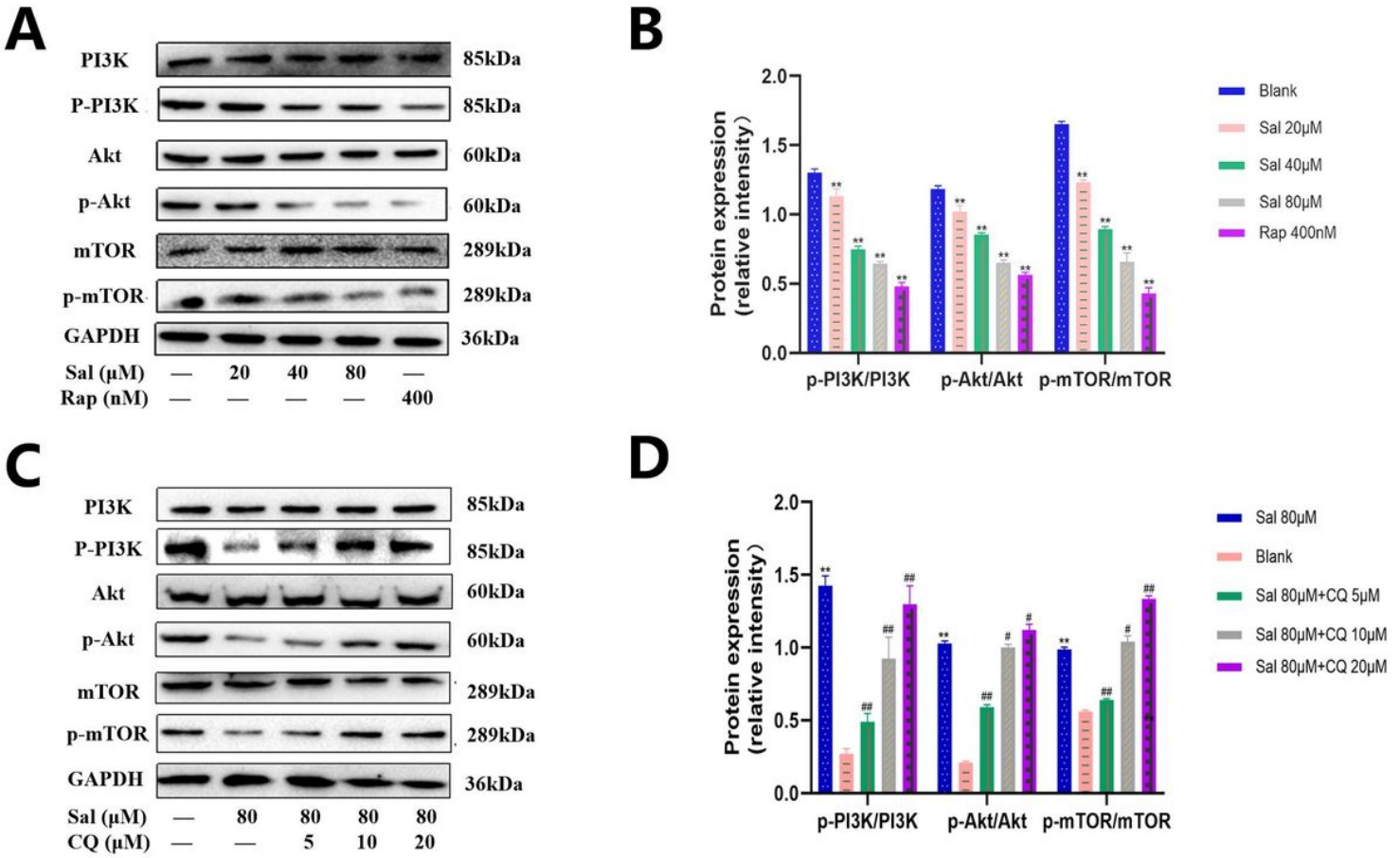

Figure 19

Expression levels of proteins associated with PI3K/AKT/mTOR signaling pathway in HepG2 cells were detected by western blot. (A) The expressions of PI3K, p-PI3K, AKT, p-AKT, mTOR and p-mTOR proteins were analyzed by western blotting in HepG2 cells induced by Sal or Rap. (B) Quantification of PI3K, p-PI3K, AKT, p-AKT, mTOR and p-mTOR proteins by the densitometry. $^{**}P<0.01$ vs. blank. (C) The expressions of PI3K, p-PI3K, AKT, p-AKT, mTOR and p-mTOR proteins were analyzed by western blotting in HepG2 cells induced by Sal and treated with CQ. (D) Quantification of PI3K, p-PI3K, AKT, p-AKT, mTOR and p-mTOR proteins by the densitometry. $^{**}P<0.01$ vs. blank. $^{\#}P<0.05$, $^{\#\#}P<0.01$ vs. Sal group. Sal, salidroside; CQ, chloroquine diphosphate.

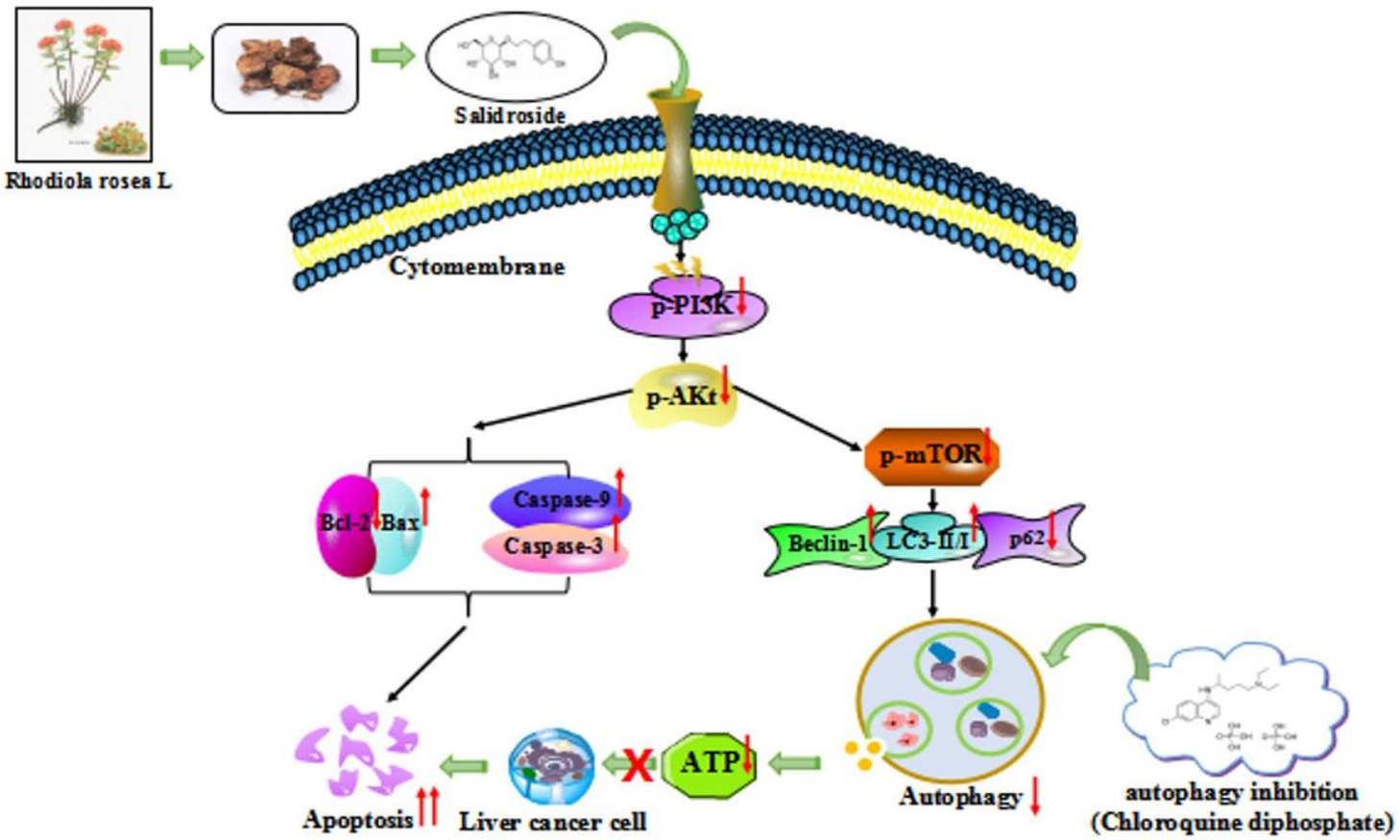

Figure 20

Schematic model revealing the potential pathway related to Sal-induced apoptosis and autophagy. Sal (a active compound extracted from the rhizome of *Rhodiola rosea* L) treatment results in mitochondrial apoptosis of HepG2 cells through PI3K-AKT signaling pathway, which damages morphology, and function. Meanwhile, Sal also regulates PI3K-AKT-mTOR signaling pathway to induce cell autophagy, thus improving cell function. Interesting, autophagy inhibitors (CQ) can not only decrese the Sal-induced autophagic flux, but also promote Sal-induced apoptosis. Sal, salidroside. CQ, chloroquine diphosphate.